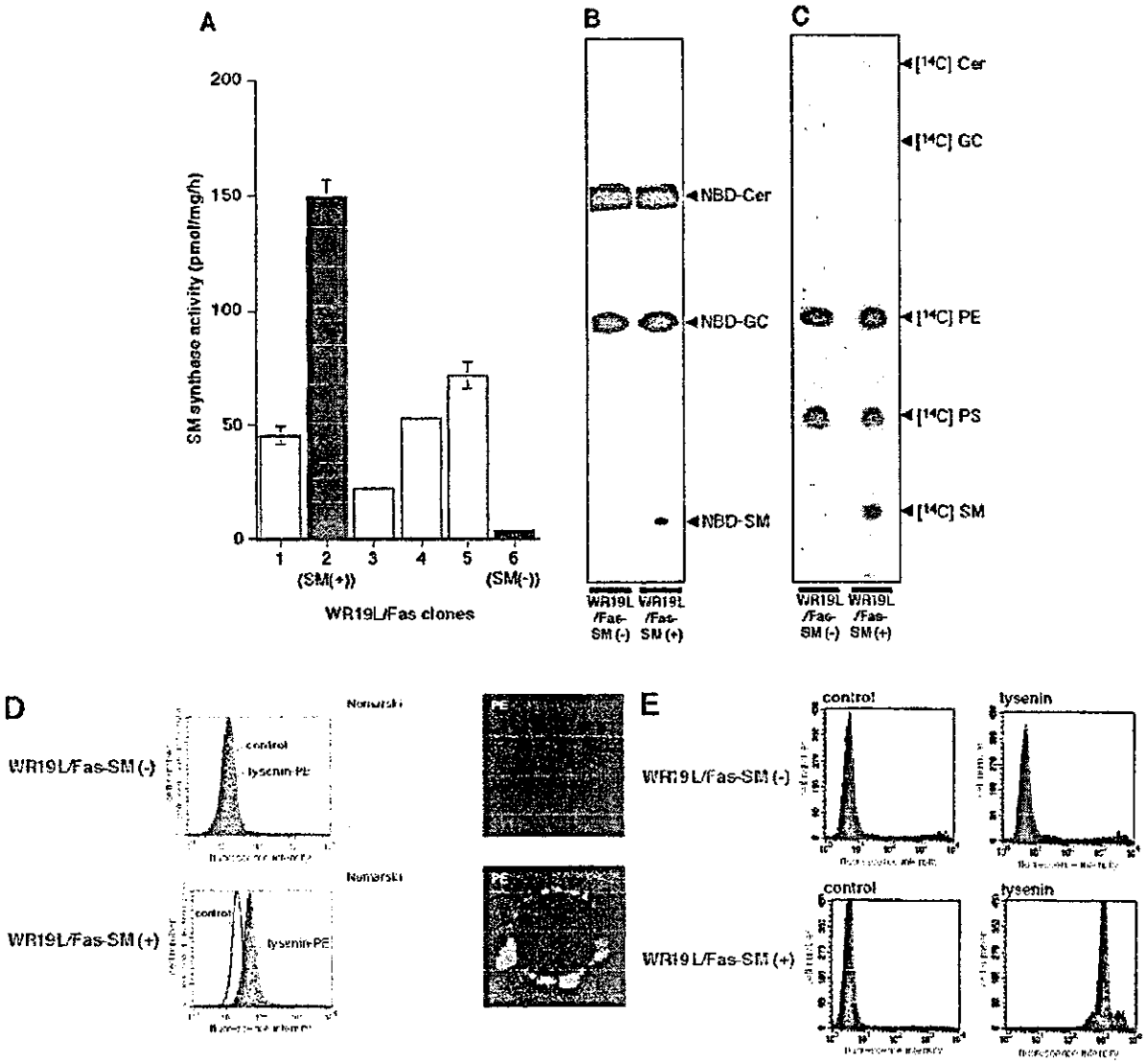

FIG. 1. **Deficiency of SM synthesis, SM synthase activity, and SM localized at the plasma membrane in the WR19L/Fas-SM(−) cells.** *A*, SM synthase activity in the cell lysates of the variant WR19L/Fas cells was assessed by the generation of C6-NBD-SM. The NBD-labeled products were quantified by a fluorospectro-photometer. *B*, SM synthase activity of WR19L/Fas-SM(−) and −SM(+). The NBD-labeled products developed on the TLC plate were visualized by a fluorospectro-photometer. The reaction was performed in the presence of 0.5 mM UDP-glucose. *Cer*, ceramide; *GC*, glucosylceramide; *C*, the cellular lipids were labeled with [^{14}C]serine, extracted by the Bligh and Dyer method, and assessed by TLC. The radiolabeled products developed on the TLC plate were visualized by BAS 2000 system. *PE*, phosphatidylethanolamine; *PS*, phosphatidylserine. *D*, SM localized at the plasma membrane was assessed by FACS analysis and confocal microscopy. FACS analysis was performed for the cells treated with the MBP-conjugated modified lysenin (*shaded* with *dark blue*) and the control cells (*unshaded*). For the results of the confocal microscopy, the fluorescence of phycoerythrin (*PE*) was pseudo-colored with *red*. *E*, The cells stained with 500 ng/ml lysenin in the presense of 20 μg/ml propidium iodide were assessed by FACS analysis. The data were the average and 1 S.D. obtained from three independent experiments (*A*) and were the representative of three independent experiments (*B–E*).

Hanada *et al.* (22) previously showed that Chinese hamster ovary cells, which express SM in the outer surface of the plasma membrane, were sensitive to lysenin-induced cell death. They also showed that reduced accumulation of SM in the variant Chinese hamster ovary cells, LY-A and LY-B, causes the significant resistance against lysenin (22). In LY-A cells, the reduction of SM is caused by the lack of non-vesicular transporter for ceramide between endoplasmic reticulum (ER) and Golgi apparatus (CERT) (26), whereas in LY-B cells, it is due to the lack of LCB1, a component of serine palmitoyltransferase (22). CERT is involved in SM synthesis by transferring ceramide from the endoplasmic reticulum to the cytoplasmic surface of Golgi apparatus (26, 31). Recently, Kobayashi and co-workers (25) reported a modified lysenin, which specifically binds to SM without the induction of cell death. By using the modified lysenin conjugated with MBP, we examined the accumulation of SM on the cellular surface of WR19L/Fas-SM(−) cells. Binding of the modified lysenin was positively detected in WR19L/Fas-SM(+) cells but not in WR19L/Fas-SM(−) cells by FACS analysis and confocal microscopy using anti-MBP antibody (Fig. 1*D*), indicating that the accumulation of SM on the outer surface of the WR19L/Fas-SM(−) cells was severely reduced. The results were supported by the fact that WR19L/Fas-SM(+) cells underwent cell death by treatment with the cytotoxic lysenin, whereas WR19L/Fas-SM(−) cells did not, when we examined cell viability by staining with propidium iodide and subsequent FACS analysis (Fig. 1*E*). These facts suggest that the severe reduction of SM at the cellular surface of WR19L/Fas-SM(−) cells is due to the lack of enzymatic activity of SM synthase.

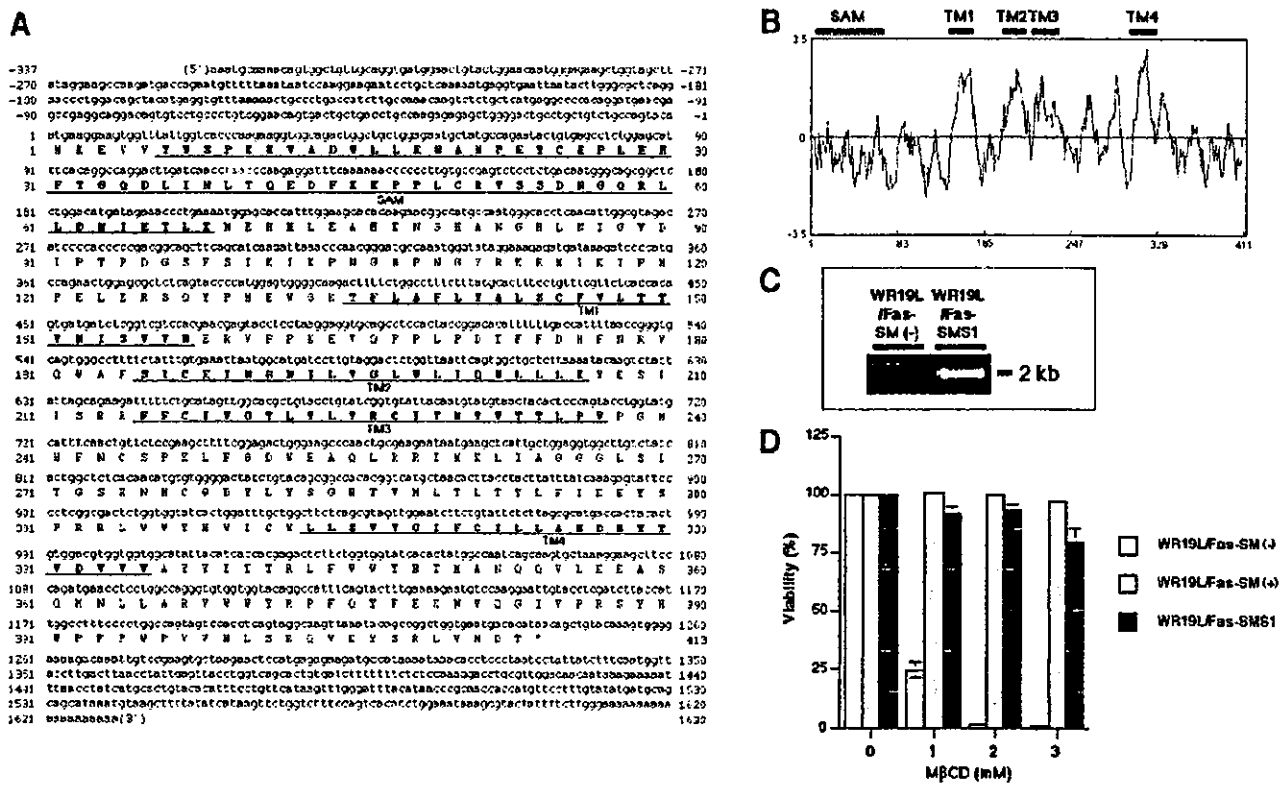

FIG. 2. **Expression cloning of a human cDNA responsible for cellular resistance to methyl-β-cyclodextrin.** *A*, nucleotide sequence and predicted amino acid sequence of SMS1. Putative SAM domain sequence and transmembrane (*TM*) regions are indicated with the *thin* and *thick underline*, respectively. SAM domain and transmembrane domains were predicted by the BLAST algorithm and SOSUI program, respectively. *B*, hydropathy plot of the amino acid sequence of SMS1 analyzed by the method of Kyte and Doolittle (45). Positions of the putative SAM domain and transmembrane regions are indicated with *horizontal bars*. *C*, integration of SMS1 cDNA (2 kb) into the genome of WR19L/Fas-SM(−) and −SMS1 cells was examined by PCR. *D*, the viability of WR19L/Fas-SM(−), −SM(+), and −SMS1 cells exposed to various concentrations of MβCD. The viability of the cells was examined using WST-8. The data were the average and 1 S.D. obtained from three independent experiments.

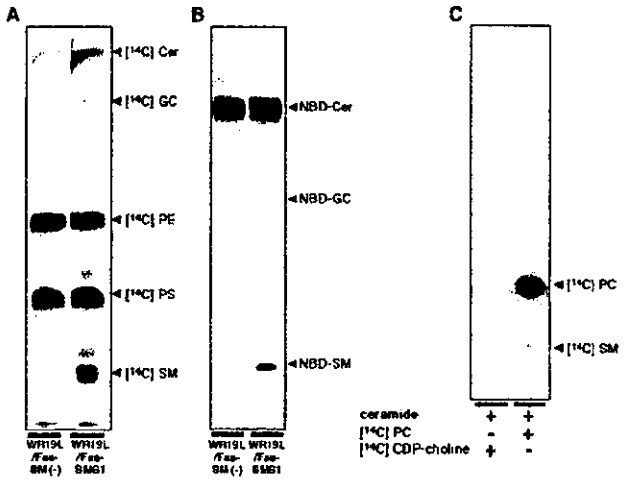

FIG. 3. **Restoration of SM synthesis and SM synthase activity in WR19L/Fas-SMS1.** *A*, the cellular lipids of WR19L/Fas-SM(−) and −SMS1 labeled with [^{14}C]serine were assessed by TLC as described in Fig. 1. *Cer*, ceramide; *GC*, glucosylceramide; *PE*, phosphatidylethanolamine; *PS*, phosphatidylserine. *B*, SM synthase activity of WR19L/Fas-SM(−) and −SMS1 cells was assessed in the absence of UDP-glucose as described in the legend for Fig. 1. *C*, SM synthase activity was assessed using the radiolabeled PC and CDP-choline as the donor of phosphocholine moiety. The radiolabeled products developed on the TLC plate were visualized by BAS 2000 system. The data were the representative of three independent experiments.

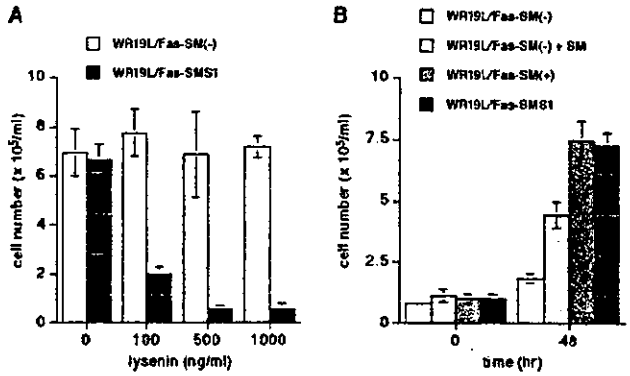

FIG. 4. **The SMS1 cDNA is essential for normal growth in mammalian lymphoid cells.** *A*, a viability assay of the WR19L/Fas-SM(−) and −SMS1 cells exposed to lysenin. After treatment with the indicated concentrations of lysenin at 37 °C for 1 h, the cell numbers were assessed by the dye exclusion method. *B*, growth of WR19L/Fas-SM(−), −SM(+), and −SMS1 cells in serum-free medium and restoration of WR19L/Fas-SM(−) cell growth by supplement of SM. The cells were incubated in serum-free medium for 48 h in the presence or absence of 50 μM SM, and the cell numbers were assessed by the dye exclusion method. The data were the average and 1 S.D. obtained from three independent experiments.

Expression Cloning of a Human cDNA Responsible for Resistance to Methyl-β-cyclodextrin-induced Cell Death—It has been reported that SM strongly interacts with cholesterol in biological and artificial membranes (28) and that SM is required to form the membrane microdomains (lipid rafts) related to cell functions such as cell death and growth (29, 30). LY-A cells were sensitive to MβCD-induced cell death due to the decrease of the SM level in plasma membrane (30). We similarly observed that WR19L/Fas-SM(−) cells were highly

sensitive to MβCD-induced cell death, whereas WR19L/Fas-SM(+) cells were not (Fig. 2*D*). This finding allowed us to screen WR19L/Fas-SM(−) cells complemented with the ability of SM synthesis using MβCD as a selective agent. Using a pantropic retroviral transfection system, WR19L/SM(−) cells were transfected with a cDNA expression library of the human HeLa cell, and the variant cells, which were resistant to MβCD due to the expression of SM in the plasma membrane, were selected. The variant cells were isolated to a single clone by a limiting dilution method. The purified cells integrated a human cDNA of 1967 bp in the genome, which encodes a peptide of 413 amino acids with 48.6 kDa of a predicted molecular mass (Fig. 2*A*). The BLAST algorithm (32) and the SOSUI program (33) suggested that this peptide carries a SAM domain in the N-terminal region and four transmembrane helices, respectively (Fig. 2*B*). The SAM domain is suggested to be involved in signal transduction, development, and transcriptional regulation (34, 35). A variety of proteins such as ephrin-related receptor tyrosine kinase, a variant of p53 (p73), and DAG kinase δ contain the SAM domain(s), which may play a role in protein-protein or protein-lipid interaction (35, 36). Recently, Huitema *et al.* (24) reported a family of SM synthases using a bioinformatics and functional cloning strategy in yeast. They identified the human cDNAs encoding the peptides that shared a sequence motif with the lipid phosphate phosphatases and Aur1p proteins required for inositolphosphorylceramide production in yeast (24). One of the human peptides, SMS1, was identical to our peptide. They further demonstrated that SMS1 was localized at Golgi apparatus and predicted the six transmembrane domains and an exoplasmic catalytic site, which is consistent with the characteristics of SM synthase suggested previously (37–39). Molecular structure of SMS1, including the transmembrane domains, should be clarified by further detailed analysis.

It was recently proposed by Luberto *et al.* (40) that the *Pseudomonas PlcH* gene product, which is a secreted protein, is a putative SM synthase. The SMS1 peptide was suggested to be an integral membrane protein and did not show any significant homology with the *PlcH* product.

The SMS1 cDNA Is Responsible for Sphingomyelin Synthase in Mammalian Cells—Huitema *et al.* (24) demonstrated the SM synthase activity in the yeast cells expressing SMS1 cDNA. Here, we demonstrated that the loss of SM synthesis in the SM-defective mammalian cells was complemented with SMS1 cDNA. WR19L/Fas-SM(−) cells transfected with SMS1 cDNA, named WR19L/Fas-SMS1 (Fig. 2*C*), restore the resistance against MβCD-induced cell death (Fig. 2*D*). Radiolabeling of cellular lipids with [^{14}C]serine revealed that [^{14}C]SM synthesis was also restored in WR19L/Fas-SMS1 cells (Fig. 3*A*), and whole cell lysate from WR19L/Fas-SMS1 cells generated C6-NBD-SM in the presence of C6-NBD-ceramide and PC (Fig. 3*B*). These results strongly suggest that the SMS1 cDNA is indispensable for SM synthase activity in mammalian cells. Furthermore, SM synthase activity in WR19L/Fas-SMS1 cells was detected in the presence of [^{14}C]PC but not [^{14}C]CDP-choline (Fig. 3*C*), suggesting that PC was a phosphocholine donor for SM synthesis by SMS1. These results indicate that the SMS1 protein possesses the characteristics consistent with those of SM synthase reported elsewhere previously (8).

The SMS1 cDNA Is Essential for Growth in Mammalian Cells—In contrast to the role of ceramide in cell death, the biological implications of SM are still ambiguous. The WR19L/Fas-SMS1 cells were sensitive to lysenin-induced cell death (Fig. 4*A*), suggesting that overexpression of SMS1 cDNA increases SM at the surface of plasma membrane. In the serum-free condition, the WR19L/Fas-SM(−) cells did not grow well, whereas the WR19L/Fas-SMS1 cells showed normal cell growth as well as the WR19L/Fas-SM(+) cells. The supplement with exogenous SM also restored cell growth of WR19L/Fas-SM(−) cells, although the growth rate was slightly reduced (Fig. 4*B*). The viable cell number of WR19L/Fas-SM(−) cells after 48 h from supplement with SM (4.4×10^5/ml) seemed to be similar to that of WR19L/Fas-SMS1 cells after 24 h (4.3×10^5/ml; data not shown), suggesting that stimulation for cell growth may be delayed due to the uptake of SM by WR19L/Fas-SM(−) cells. These observations suggest that SM synthesis through SM synthase is essential for cell growth. Huitema *et al.* (24) suggested that SMS2 is localized at the plasma membrane and may play a role in signal transduction. Here, we demonstrated that the cell growth was closely related with the accumulation of SM at the plasma membrane caused by SMS1, suggesting that SMS1 may be involved in signal transduction for cell growth as well as SMS2. In contrast to our observation, it has been reported that the variant melanoma cells deficient in glucosylceramide synthase showed no significant difference of cell growth as compared with the original cells (41), although glucosylceramide is an essential lipid for the diversity of glycosphingolipids. One possible explanation for the difference between SM and glucosylceramide is the significant involvement of SM in the microdomains responsible for various cell signaling events.

SM synthase regulates the levels of pro-apoptotic ceramide and anti-apoptotic DAG in an opposite manner and balances the levels of phospholipid PC and sphingolipid SM (9). SM synthase is closely regulated by the levels of ceramide and DAG, as well as extracellular stresses (15, 18, 31, 42). SM synthase is suggested to localize not only in the plasma membrane (37) and Golgi apparatus (43) but also in the endoplasmic reticulum (38) and nucleus (17, 44). We recently reported that, in Fas-induced Jurkat T cell apoptosis, ceramide increased through inhibition of SM synthase in the nucleus (17). The relationship between the intracellular localization and the regulation of SM synthase activity and the regulatory mechanism for the levels of lipid mediators in cell growth and death through SM synthase should be clarified by detailed analysis of the *SMS* genes.

Acknowledgments—We appreciate Dr. K. Hanada (National Institute of Infectious Diseases) for a useful support in terms of retroviral transfection and MβCD screening methods and Drs. Y. Hirabayashi (RIKEN) and Y. Igarashi (Hokkaido University) for careful discussions. We also appreciate Drs. A. Takaori and M. Kobayashi (Kyoto University) for a technical advice for retroviral transfection.

REFERENCES

1. English, D. (1996) *Cell. Signal.* **8**, 341–347
2. Majerus, P. W. (1992) *Annu. Rev. Biochem.* **61**, 225–250
3. Pettus, B. J., Chalfant, C. E., and Hannun, Y. A. (2002) *Biochim. Biophys. Acta* **1585**, 114–125
4. Okazaki, T., Kondo, T., Kitano, T., and Tashima, M. (1998) *Cell. Signal.* **10**, 685–692
5. Hannun, Y. A. (1994) *J. Biol. Chem.* **269**, 3125–3128
6. Moschetta, A., Portincasa, P., van Erpecum, K. J., Debellis, L., Vanberge-Henegouwen, G. P., and Palasciano, G. (2003) *Dig. Dis. Sci.* **48**, 1094–1101
7. Dillehay, D. L., Webb, S. K., Schmelz, E. M., and Merrill, A. H., Jr. (1994) *J. Nutr.* **124**, 615–620
8. Voelker, D. R., and Kennedy, E. P. (1982) *Biochemistry* **21**, 2753–2759
9. Hampton, R. Y., and Morand, O. H. (1989) *Science* **246**, 1050
10. Pagano, R. E. (1988) *Trends Biochem. Sci.* **13**, 202–205
11. Moscat, J., Cornet, M. E., Diaz-Meco, M. T., Larrodera, P., Lopez-Alanon, D., and Lopez-Barahona, M. (1989) *Biochem. Soc. Trans.* **17**, 988–991
12. Lucas, L., del Peso, L., Rodriguez, P., Penalva, V., and Lacal, J. C. (2000) *Oncogene* **19**, 431–437
13. Hannun, Y. A., and Bell, R. M. (1989) *Science* **243**, 500–507
14. Miro-Obradors, M. J., Osada, J., Aylagas, H., Sanchez-Vegazo, I., and Palacios-Alaiz, E. (1993) *Carcinogenesis* **14**, 941–946
15. Riboni, L., Tettamanti, G., and Viani, P. (2002) *Cerebellum* **1**, 129–135
16. Luberto, C., and Hannun, Y. A. (1998) *J. Biol. Chem.* **273**, 14550–14559
17. Watanabe, M., Kitano, T., Kondo, T., Yabu, T., Taguchi, Y., Tashima, M., Umehara, H., Domae, N., Uchiyama, T., and Okazaki, T. (2004) *Cancer Res.* **64**, 1–8
18. Itoh, M., Kitano, T., Watanabe, M., Kondo, T., Yabu, T., Taguchi, Y., Iwai, K., Tashima, M., Uchiyama, T., and Okazaki, T. (2003) *Clin. Cancer Res.* **9**,

415–423
19. Okazaki, T., Bell, R. M., and Hannun, Y. A. (1989) *J. Biol. Chem.* **264,** 19076–19080
20. Chatterjee, S. (1999) *Chem. Phys. Lipids* **102,** 79–96
21. Cremesti, A. E., Goni, F. M., and Kolesnick, R. (2002) *FEBS Lett.* **531,** 47–53
22. Hanada, K., Hara, T., Fukasawa, M., Yamaji, A., Umeda, M., and Nishijima, M. (1998) *J. Biol. Chem.* **273,** 33787–33794
23. Shakor, A. B., Czurylo, E. A., and Sobota, A. (2003) *FEBS Lett.* **542,** 1–6
24. Huitema, K., van den Dikkenberg, J., Brouwers, J. F. H. M., and Holthuis, J. C. M. (2004) *EMBO J.* **23,** 33–44
25. Yamaji-Hasegawa, A., Makino, A., Baba, T., Senoh, Y., Kimura-Suda, H., Sato, S. B., Terada, N., Ohno, S., Kiyokawa, E., Umeda, M., and Kobayashi, T. (2003) *J. Biol. Chem.* **278,** 22762–22770
26. Hanada, K., Kumagai, K., Yasuda, S., Miura, Y., Kawano, M., Fukasawa, M., and Nishijima, M. (2003) *Nature* **426,** 803–809
27. Yamaji, A., Sekizawa, Y., Emoto, K., Sakuraba, H., Inoue, K., Kobayashi, H., and Umeda, M. (1998) *J. Biol. Chem.* **273,** 5300–5306
28. Slotte, J. P. (1999) *Chem. Phys. Lipids* **102,** 13–27
29. Ostermeyer, A. G., Beckrich, B. T., Ivarson, K. A., Grove, K. E., and Brown, D. A. (1999) *J. Biol. Chem.* **274,** 34459–34466
30. Fukasawa, M., Nishijima, M., Itabe, H., Takano, T., and Hanada, K. (2000) *J. Biol. Chem.* **275,** 34028–34034
31. Fukasawa, M., Nishijima, M., and Hanada, K. (1999) *J. Cell Biol.* **144,** 673–685
32. Altschul, S. F., Gish, W., Miller, W., Myers, E. W., and Lipman, D. J. (1990) *J. Mol. Biol.* **215,** 403–410
33. Hirokawa, T., Boon-Chieng, S., and Mitaku, S. (1998) *Bioinformatics (Oxf.)* **14,** 378–379
34. Bork, P., and Koonin, E. V. (1998) *Nat. Genet.* **18,** 313–318
35. Barrera, F. N., Poveda, J. A., Gonzalez-Ros, J. M., and Neira, J. L. (2003) *J. Biol. Chem.* **278,** 46878–46885
36. Schultz, J., Ponting, C. P., Hofmann, K., and Bork, P. (1997) *Protein Sci.* **6,** 249–253
37. Futerman, A. H., Stieger, B., Hubbard, A. L., and Pagano, R. E. (1990) *J. Biol. Chem.* **265,** 8650–8657
38. van Helvoort, A., Stoorvogel, W., van Meer, G., and Burger, N. J. (1997) *J. Cell Sci.* **110,** 781–788
39. Elmendorf, H. G., and Haldar, K. (1994) *J. Cell Biol.* **124,** 449–462
40. Luberto, C., Stonehouse, M. J., Collins, E. A., Marchesini, N., El-Bawab, S., Vasil, A. I., Vasil, M. L., and Hannun, Y. A. (2003) *J. Biol. Chem.* **278,** 32733–32743
41. Ichikawa, S., Nakajo, N., Sakiyama, H., and Hirabayashi, Y. (1994) *Proc. Natl. Acad. Sci. U. S. A.* **91,** 2703–2707
42. Hanada, K., Horii, M., and Akamatsu, Y. (1991) *Biochim. Biophys. Acta* **1086,** 151–156
43. Allan, D., and Obradors, M. J. (1999) *Biochim. Biophys. Acta* **1450,** 277–287
44. Albi, E., and Magni, M. V. (1999) *FEBS Lett.* **460,** 369–372
45. Kyte, J., and Doolittle, R. F. (1982) *J. Mol. Biol.* **157,** 105–132

Peyer's Patch Dendritic Cells Capturing Oral Antigen Interact with Antigen-Specific T Cells and Induce Gut-Homing $CD4^+CD25^+$ Regulatory T Cells in Peyer's Patches

KATSUYA NAGATANI, KAYO SAGAWA, YOSHINORI KOMAGATA, AND KAZUHIKO YAMAMOTO

Department of Allergy and Rheumatology, Graduate School of Medicine, University of Tokyo, Tokyo, Japan

ABSTRACT: Antigen-specific naive T cells accumulated in Peyer's patches only after the feeding of antigen. DCs that captured oral antigen interacted with these T cells in the IFR of PP. Some of these T cells acquired a similar phenotype to $CD4^+$ $CD25^+$ regulatory T cells and $CCR9^+$ gut-homing T cells.

KEYWORDS: Peyer's patch; dendritic cell; chemokine receptor; regulatory T cell

INTRODUCTION

It is thought that antigen-specific regulatory T cells are generated in the gut-associated lymphoid tissue (GALT), including Peyer's patches (PPs), after antigen is orally administered. However, the importance of dendritic cells (DCs) in the generation of regulatory T cells, and the kind of regulatory T cells generated in PPs are still unclear. Here, we show that PP DCs capturing oral antigen interacted with antigen-specific T cells and induced gut-homing $CD4^+CD25^+$ regulatory T cells in PPs.

MATERIALS AND METHODS

We transferred naive T cells of ovalbumin (OVA)-TCR transgenic mice (DO11.10) into BALB/c mice, which were then fed FITC-conjugated OVA (FITC-OVA) (30 mg/mouse) 24 h later. Kinetics of oral antigen–loaded cells and interaction between antigen-specific T cells and antigen-loaded DCs in PPs after the feeding of OVA (or FITC-OVA) were checked by immunofluorescence staining.

Address for correspondence: Yoshinori Komagata, Department of Allergy and Rheumatology, Graduate School of Medicine, University of Tokyo, 7-3-1 Hongo, Bunkyo-ku, Tokyo 113-8655, Japan. Voice: +81-3-3815-5411, ext. 37263; fax: +81-3-3815-5954.
komagata-tky@umin.ac.jp

Ann. N.Y. Acad. Sci. 1029: 366–370 (2004).
doi: 10.1196/annals.1309.020

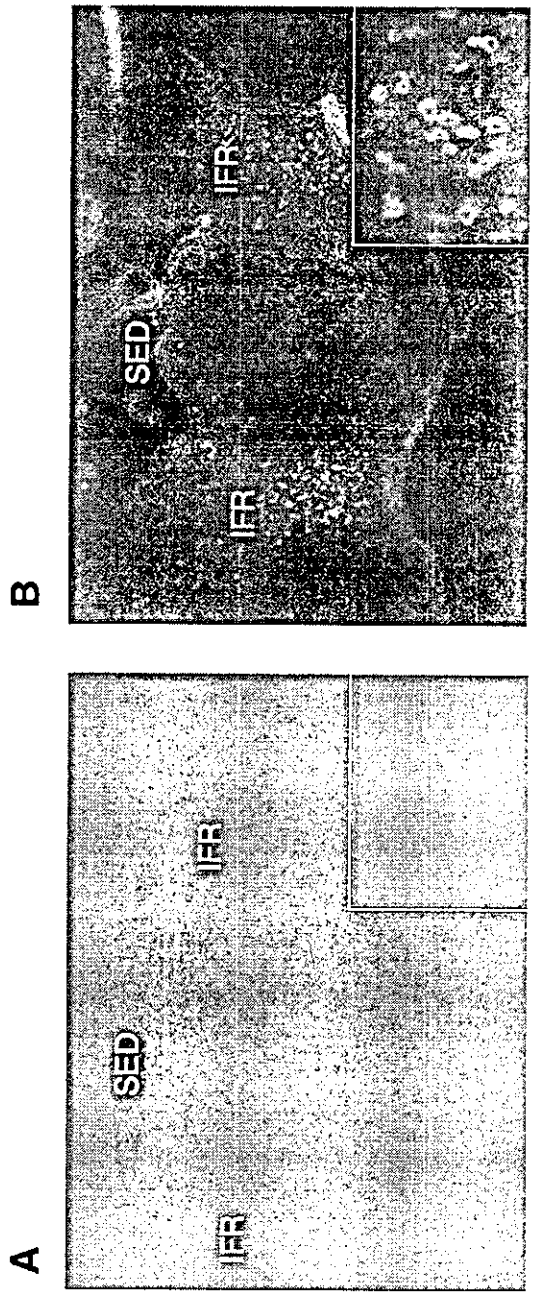

FIGURE 1. OVA-specific T cells accumulated in IFR of Peyer's patch by OVA feeding. We transferred OVA-specific T cells of DO11.10 mice into naive BALB/c mice, then fed 30 mg OVA to these mice. We collected Peyer's patches 24 h after the transfer and stained with FITC anti-KJ1.26 antibody. (A) Peyer's patch of nonfed mouse. OVA-specific T cells are not detected (inset magnified ×200). (B) Peyer's patch of OVA-fed mouse. OVA-specific T cells accumulated in IFR (inset magnified ×200).

FIGURE 2. FITC-OVA–loaded DCs interact with OVA-specific T cells in IFR of Peyer's patches. (**A**) We transferred OVA-specific T cells of DO11.10 mice into naive BALB/c mice, then fed 30 mg of FITC-conjugated OVA (FITC-OVA) to these mice. We collected Peyer's patches 24 h after the transfer, and stained with FITC anti-KJ1.26 antibody and PE anti-CD11c antibody. (IFR, interfollicular region; SED, subepithelial dome; magnified ×40). (**B**) FITC-OVA–loaded DCs (*closed arrows*) contact OVA-specific T cells (*open arrows*) in IFR after FITC-OVA feeding (magnified ×400).

To examine the phenotype of OVA-specific T cells accumulated in PPs after OVA feeding, we purified KJ1.26 positive T cells from PPs by magnetic beads (MACS, Miltenyi Biotec, Bergisch Gladbach, Germany) and checked relative gene expression by real-time RT-PCR (iCycler iQ; Bio-Rad, CA).

RESULTS

FITC-positive cells appeared in the subepithelial dome (SED) of PPs as early as three hours after the feeding of FITC-OVA. Double staining with PE anti-CD11c antibody showed that FITC-positive cells in SEDs were CD11c-positive DCs (data not shown). Twenty-four hours after the feeding of FITC-OVA, DCs capturing FITC-OVA migrated from the SED to the interfollicular region (IFR) and interacted with OVA-specific T cells accumulated in the IFR of PPs (FIG. 1B and FIG. 2). In contrast, OVA-specific T cells were not detected in IFRs in nonfed mice (FIG. 1A).

We investigated the gene expression levels of chemokine receptors such as CCR4, CCR7, CCR8, CCR9, and CXCR3 in OVA-specific T cells by quantitative

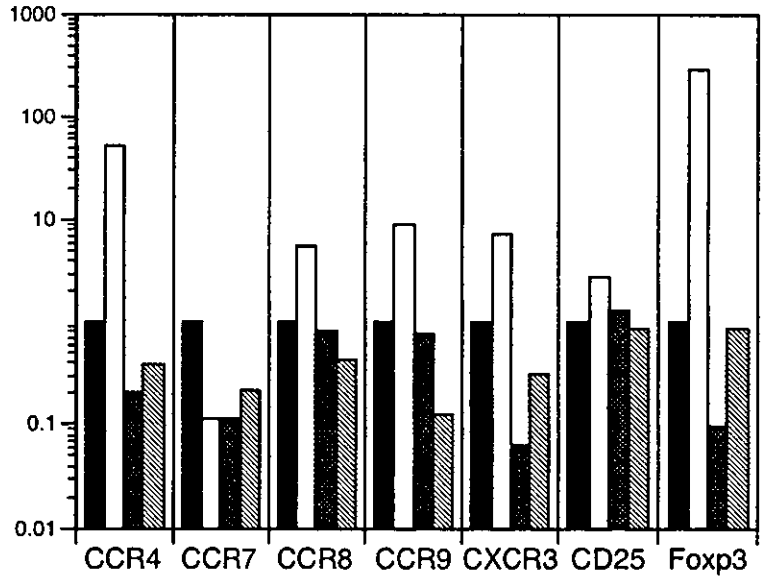

FIGURE 3. Gene expression in OVA-specific T cells accumulating in Peyer's patches after OVA feeding. We transferred OVA-specific T cells of DO11.10 mice into naive BALB/c mice, followed by feeding of 30 mg OVA. Twenty-four hours after the transfer, KJ1.26-positive OVA-specific T cells were purified from Peyer's patches, and total RNA was extracted. We checked relative gene expression of OVA-specific T cells accumulated in Peyer's patch by quantitative real time RT-PCR (*open box*). As controls, KJ1.26-positive T cells from spleens of OVA-fed (*black box with white dots*), nonfed mice (*striped box*), and KJ1.26-positive T cells before transfer (*black box*) were also checked.

real-time PCR. Gene expression of CCR4, CCR8, CCR9, and CXCR3 was substantially higher in OVA-specific T cells accumulated in PPs after OVA feeding (FIG. 3).

It has been reported that CCR4 and CCR8 are expressed on $CD4^+CD25^+$ regulatory T cells.[1] Therefore, we next checked the gene expression of Foxp3, which is a $CD4^+CD25^+$ regulatory T cell–specific transcription factor,[2] in OVA-specific T cells. Surprisingly, the Foxp3 gene level in OVA-specific T cells accumulated in PPs after OVA feeding was 294-fold more abundant than in OVA-specific T cells before the transfer. Expression of CCR7, which is regarded as a marker of naive T cells, in the OVA-specific T cells before the transfer, was relatively high (FIG. 3).

DISCUSSION

Recent studies have shown that CCR4, CCR8, and CXCR3 are expressed on $CD4^+CD25^+$ regulatory T cells and that Foxp3 is exclusively expressed in these T cells.[1,2] In addition, CCR9 has been reported to be expressed by gut-homing T cells.[3] These results suggest that DCs that capture oral antigens in the SED migrate into the IFR and interact with antigen-specific T cells, and that some antigen-specific T cells acquire a similar phenotype to $CCR9^+$ gut-homing T cells and $CD4^+CD25^+$ regulatory T cells.

REFERENCES

1. IELLEM, A., M. MARIANI, R. LANG, *et al.* 2001. Unique chemotactic response profile and specific expression of chemokine receptors CCR4 and CCR8 by $CD4^+CD25^+$ regulatory T cells. J. Exp. Med. **194:** 847–854.
2. HORI, S., T. NOMURA & S. SAKAGUCHI. 2003. Control of regulatory T cell development by the transcription factor Foxp3. Science **299:** 1057–1061.
3. ZABEL, B.A., W.W. AGACE, J.J. CAMPBELL, *et al.* 1999. Human G protein–coupled receptor GPR-9-6/CC chemokine receptor 9 is selectively expressed on intestinal homing T lymphocytes, mucosal lymphocytes, and thymocytes and is required for thymus-expressed chemokine–mediated chemotaxis. J. Exp. Med. **190:** 1241–1256.

(Qiagen). Semi-quantitative RT–PCR was performed using a nested protocol as described by ref. 11. Positive control RNA was provided by C. Drosten (Bernhard Nocht Institute for Tropical Medicine, National Reference Center for Tropical Diseases). Virus titration was performed by seeding 5×10^5 Vero E6 cells per well in 96-well microtitre plates 1 day before infection. Culture supernatant from infected 293T cells was added to the first set of wells in triplicate and serially diluted. Cells were monitored for CPE 3 days after infection of Vero E6 cells. The effect of affinity-purified goat anti-ACE1 or -ACE2 antibody on SARS-CoV-induced cytopathicity was measured by reading absorbance at 492 nm of cells incubated with CellTiter 96 (Promega).

Received 14 September; accepted 23 October 2003; doi:10.1038/nature02145.

1. Gallagher, T. M. & Buchmeier, M. J. Coronavirus spike proteins in viral entry and pathogenesis. *Virology* 279, 371–374 (2001).
2. Holmes, K. V. SARS-associated coronavirus. *N. Engl. J. Med.* 348, 1948–1951 (2003).
3. Donoghue, M. *et al.* A novel angiotensin-converting enzyme-related carboxypeptidase (ACE2) converts angiotensin I to angiotensin 1–9. *Circ. Res.* 87, E1–E9 (2000).
4. Tipnis, S. R. *et al.* A human homolog of angiotensin-converting enzyme. Cloning and functional expression as a captopril-insensitive carboxypeptidase. *J. Biol. Chem.* 275, 33238–33243 (2000).
5. Holmes, K. V. *et al.* Coronavirus receptor specificity. *Adv. Exp. Med. Biol.* 342, 261–266 (1993).
6. Dveksler, G. S. *et al.* Several members of the mouse carcinoembryonic antigen-related glycoprotein family are functional receptors for the coronavirus mouse hepatitis virus-A59. *J. Virol.* 67, 1–8 (1993).
7. Delmas, B. *et al.* Aminopeptidase N is a major receptor for the entero-pathogenic coronavirus TGEV. *Nature* 357, 417–420 (1992).
8. Tresnan, D. B. & Holmes, K. V. Feline aminopeptidase N is a receptor for all group I coronaviruses. *Adv. Exp. Med. Biol.* 440, 69–75 (1998).
9. Yeager, C. L. *et al.* Human aminopeptidase N is a receptor for human coronavirus 229E. *Nature* 357, 420–422 (1992).
10. Ksiazek, T. G. *et al.* A novel coronavirus associated with severe acute respiratory syndrome. *N. Engl. J. Med.* 348, 1953–1966 (2003).
11. Drosten, C. *et al.* Identification of a novel coronavirus in patients with severe acute respiratory syndrome. *N. Engl. J. Med.* 348, 1967–1976 (2003).
12. Kuiken, T. *et al.* Newly discovered coronavirus as the primary cause of severe acute respiratory syndrome. *Lancet* 362, 263–270 (2003).
13. Fouchier, R. A. *et al.* Aetiology: Koch's postulates fulfilled for SARS virus. *Nature* 423, 240 (2003).
14. Rota, P. A. *et al.* Characterization of a novel coronavirus associated with severe acute respiratory syndrome. *Science* 300, 1394–1399 (2003).
15. Marra, M. A. *et al.* The Genome sequence of the SARS-associated coronavirus. *Science* 300, 1399–1404 (2003).
16. Sturman, L. S. & Holmes, K. V. Proteolytic cleavage of peplomeric glycoprotein E2 of MHV yields two 90K subunits and activates cell fusion. *Adv. Exp. Med. Biol.* 173, 25–35 (1984).
17. Jackwood, M. W. *et al.* Spike glycoprotein cleavage recognition site analysis of infectious bronchitis virus. *Avian Dis.* 45, 366–372 (2001).
18. Spaan, W., Cavanagh, D. & Horzinek, M. C. Coronaviruses: structure and genome expression. *J. Gen. Virol.* 69, 2939–2952 (1988).
19. Bonavia, A., Zelus, B. D., Wentworth, D. E., Talbot, P. J. & Holmes, K. V. Identification of a receptor-binding domain of the spike glycoprotein of human coronavirus HCoV-229E. *J. Virol.* 77, 2530–2538 (2003).
20. Breslin, J. J. *et al.* Human coronavirus 229E: receptor binding domain and neutralization by soluble receptor at 37 degrees C. *J. Virol.* 77, 4435–4438 (2003).
21. Kubo, H., Yamada, Y. K. & Taguchi, F. Localization of neutralizing epitopes and the receptor-binding site within the amino-terminal 330 amino acids of the murine coronavirus spike protein. *J. Virol.* 68, 5403–5410 (1994).
22. Komatsu, T. *et al.* Molecular cloning, mRNA expression and chromosomal localization of mouse angiotensin-converting enzyme-related carboxypeptidase (mACE2). *DNA Seq.* 13, 217–220 (2002).
23. Harmer, D., Gilbert, M., Borman, R. & Clark, K. L. Quantitative mRNA expression profiling of ACE 2, a novel homologue of angiotensin converting enzyme. *FEBS Lett.* 532, 107–110 (2002).
24. Choe, H. *et al.* The beta-chemokine receptors CCR3 and CCR5 facilitate infection by primary HIV-1 isolates. *Cell* 85, 1135–1148 (1996).
25. Leung, W. K. *et al.* Enteric involvement of severe acute respiratory syndrome-associated coronavirus infection. *Gastroenterology* 125, 1011–1017 (2003).
26. Crackower, M. A. *et al.* Angiotensin-converting enzyme 2 is an essential regulator of heart function. *Nature* 417, 822–828 (2002).
27. Vickers, C. *et al.* Hydrolysis of biological peptides by human angiotensin-converting enzyme-related carboxypeptidase. *J. Biol. Chem.* 277, 14838–14843 (2002).
28. Delmas, B. *et al.* Determinants essential for the transmissible gastroenteritis virus-receptor interaction reside within a domain of aminopeptidase-N that is distinct from the enzymatic site. *J. Virol.* 68, 5216–5224 (1994).
29. Huang, L. *et al.* Novel peptide inhibitors of angiotensin-converting enzyme 2. *J. Biol. Chem.* 278, 15532–15540 (2003).
30. Dales, N. A. *et al.* Substrate-based design of the first class of angiotensin-converting enzyme-related carboxypeptidase (ACE2) inhibitors. *J. Am. Chem. Soc.* 124, 11852–11853 (2002).

Supplementary Information accompanies the paper on **www.nature.com/nature**.

Acknowledgements We thank J. Coderre for assistance with RT–PCR, M. Kirk for editing, and S. H. Wang, E. Kieff, J. Sodroski, C. Gerard and N. Gerard for guidance and helpful conversations.

Competing interests statement The authors declare that they have no competing financial interests.

Correspondence and requests for materials should be addressed to H.C. (hyeryun.choe@tch.harvard.edu) or M.F. (farzan@mbcrr.harvard.edu).

Altered thymic T-cell selection due to a mutation of the ZAP-70 gene causes autoimmune arthritis in mice

Noriko Sakaguchi[1,2]*, Takeshi Takahashi[1]*, Hiroshi Hata[1], Takashi Nomura[1], Tomoyuki Tagami[1], Sayuri Yamazaki[1], Toshiko Sakihama[1], Takaji Matsutani[3], Izumi Negishi[4], Syuichi Nakatsuru[1] & Shimon Sakaguchi[1,2]

[1]*Department of Experimental Pathology, Institute for Frontier Medical Sciences, Kyoto University, Kyoto 606-8507, Japan*
[2]*Laboratory for Immunopathology, RIKEN Research Center for Allergy and Immunology, Yokohama 230-0045, Japan*
[3]*Department of Immunology, Shionogi Institute for Medical Science, Settsu, Osaka 566-0022, Japan*
[4]*Department of Dermatology, Gunma University Hospital, Maebashi, Gunma 371-8511, Japan*

* These authors contributed equally to this work

Rheumatoid arthritis (RA), which afflicts about 1% of the world population, is a chronic systemic inflammatory disease of unknown aetiology that primarily affects the synovial membranes of multiple joints[1–3]. Although $CD4^+$ T cells seem to be the prime mediators of RA, it remains unclear how arthritogenic $CD4^+$ T cells are generated and activated[1–3]. Given that highly self-reactive T-cell clones are deleted during normal T-cell development in the thymus, abnormality in T-cell selection has been suspected as one cause of autoimmune disease[4,5]. Here we show that a spontaneous point mutation of the gene encoding an SH2 domain of ZAP-70, a key signal transduction molecule in T cells[6], causes chronic autoimmune arthritis in mice that resembles human RA in many aspects. Altered signal transduction from T-cell antigen receptor through the aberrant ZAP-70 changes the thresholds of T cells to thymic selection, leading to the positive selection of otherwise negatively selected autoimmune T cells. Thymic production of arthritogenic T cells due to a genetically determined selection shift of the T-cell repertoire towards high self-reactivity might also be crucial to the development of disease in a subset of patients with RA.

The SKG strain, which spontaneously develops chronic arthritis, is derived from our closed breeding colony of BALB/c mice. Joint swelling with hyperaemia became macroscopically evident in SKG mice at about 2 months of age, initially at a few interphalangeal joints of the forepaws, then progressing in a symmetrical fashion to swelling of other finger joints of the forepaws and hindpaws, and larger joints (wrists and ankles) (Fig. 1a–d). Knee, elbow, shoulder or vertebral joints were rarely affected except for the joint at the base of the tail in aged SKG mice (Fig. 1e). Radiographic examination revealed destruction and fusion of the subchondral bones, joint dislocation, and osteoporosis by 8–12 months of age (Fig. 1f–i). Despite suffering from such severe chronic arthritis, most SKG mice survived well to 1 year of age, generally with more severe arthritides in females (Fig. 1j).

Histology of the swollen joints showed severe synovitis with massive subsynovial infiltration of neutrophils, lymphocytes, macrophages and plasma cells, villus proliferation of synoviocytes accompanying pannus formation and neovascularization, and neutrophil-rich exudates in the joint cavity (Fig. 1k, l), with progression of synoviocyte proliferation, pannus-eroded adjacent cartilage and subchondral bone. Immunohistochemical staining revealed that $CD4^+$ T cells predominantly infiltrated the subsynovial tissue (Fig. 1m, n). As extra-articular manifestations of the disease, most (more than 90%) mice older than 6 months of age developed interstitial pneumonitis with various degrees of perivascular and

peribronchiolar cellular infiltration (Fig. 1o); more than 90% showed infiltration of inflammatory cells in the skin (Supplementary Fig. 1a). Some (10–20%) mice had subcutaneous necrobiotic nodules, not unlike rheumatoid nodules in RA (Fig. 1p), and vasculitides (Supplementary Fig. 1b). SKG mice did not show lymphoadenopathy or lupus-like diseases (such as immune-complex glomerulonephritis).

SKG mice developed high titres of rheumatoid factor (RF), autoantibodies specific for type II collagen, antibodies reactive with heat shock protein (HSP)-70 of *Mycobacterium tuberculosis* presumably due to a cross-reaction with a conserved epitope of HSP, severe hypergammaglobulinaemia and a high concentration of the circulating immune complexes. However, there were no significant titres of anti-DNA antibodies or organ-specific autoantibodies such as those specific for thyroglobulins or gastric parietal cells[1–3,7] (Fig. 1q–v).

Thus, this spontaneous arthritis in SKG mice resembles RA in clinical and histological characteristics of articular and extra-articular lesions and in serological features[1–3].

Transfer of spleen and lymph node T cells, $CD4^+$ T cells in particular, from arthritic SKG mice produced similar arthritis in

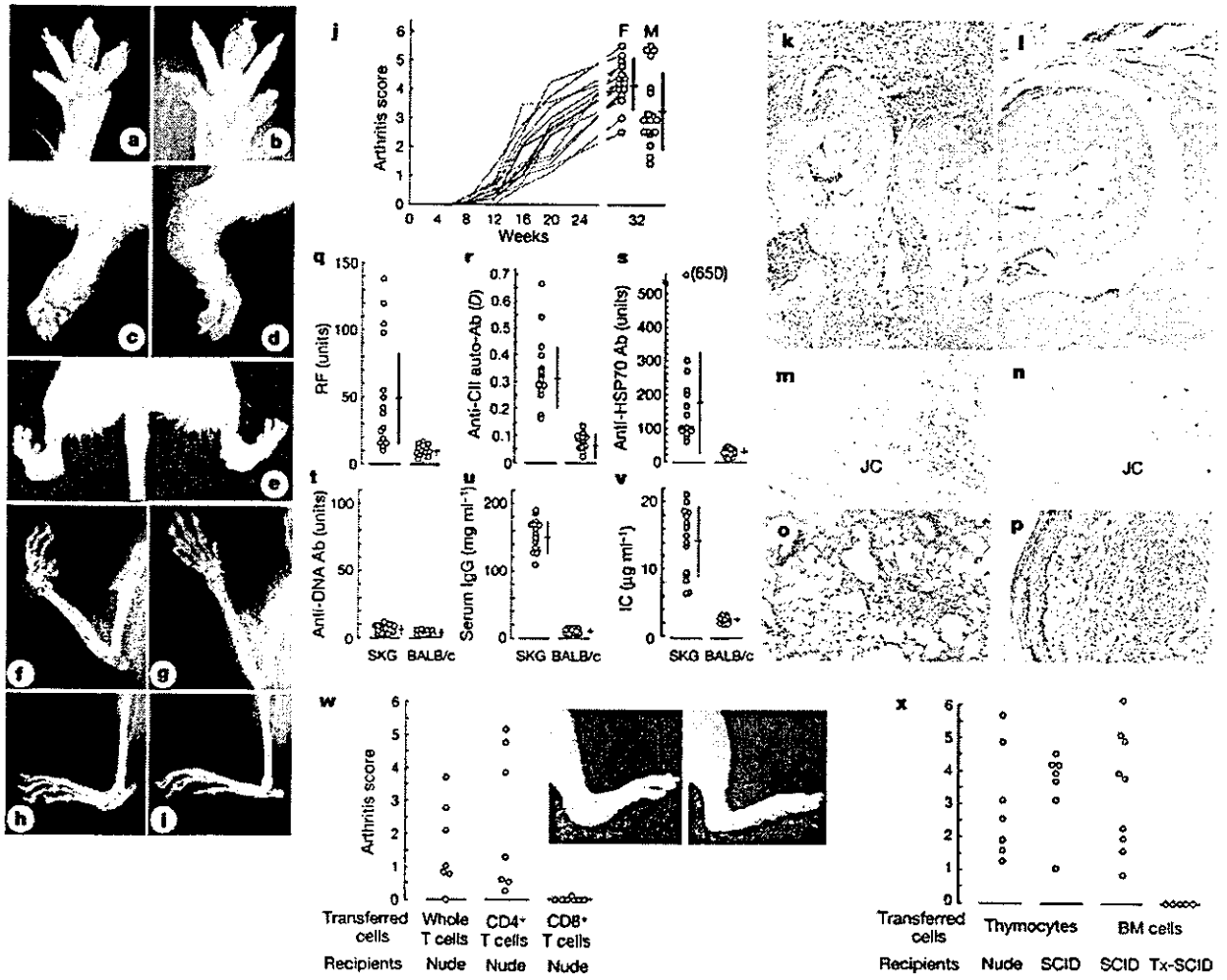

Figure 1 Arthritis in SKG mice. **a–e**, Swelling of joints: fingers (**a**) and toes (**b**) of a 4-month-old SKG mouse; forepaw (**c**) and hindpaw (**d**) of a 6-month-old SKG mouse; deformity of bilateral ankles and swelling of the base of the tail (**e**) in an 18-month-old SKG mouse. **f–i**, X-ray photographs of joints: wrist (**f**) and ankle (**h**) of an 8-month-old SKG mouse, and wrist (**g**) and ankle (**i**) of an 8-month-old BALB/c mouse. **j**, Time course of joint swelling in female SKG mice, and arthritis scores of 8-month-old female (F) and male (M) SKG mice ($n = 15$ each). Vertical bars represent s.e.m. See Methods for details on the scoring of joint swelling. **k–p**, Histology of arthritis and extra-articular lesions in SKG mice: a finger joint of a 6-month-old SKG (**k**) or BALB/c mouse (**l**) (haematoxylin/eosin (HE) staining, original magnification ×40); immunoperoxidase staining of synovial tissue in a finger joint of a 3-month-old SKG mouse with anti-CD4 mAb (GK1.5) (**m**) or anti-CD8 mAb (3–155) (**n**) (magnification ×40) (JC, joint cavity); interstitial pneumonitis (**o**) and a rheumatoid nodule-like lesion (**p**) in an 8-month-old SKG mouse (HE staining, magnification ×40). **q–v**, Serological characteristics of SKG mice: RF (**q**), anti-CII Ab (**r**), anti-HSP70 antibody (Ab) (**s**), anti-DNA antibody (**t**), concentration of IgG (**u**) and immune complexes (**v**) in the sera from 6-month-old female SKG or BALB/c mice ($n = 15$ each). **w**, Adoptive transfer of arthritis. The same dose (2.5×10^7) of whole, $CD4^+$ or $CD8^+$ T cells prepared from lymph nodes and spleens of arthritis-bearing 6-month-old SKG mice were transferred to 6-week-old BALB/c nude mice (SLC, Shizuoka). Inset, swelling of a hindpaw (left) and an intact paw (right) of a nude mouse transferred with $CD4^+$ T cells and with $CD8^+$ T cells, respectively. **x**, Thymocytes (10^8) or T-cell-depleted bone marrow cell suspensions (5×10^6) from the same SKG mice were transferred to 6-week-old nude or C.B.-17 SCID mice (Clea, Tokyo) or SCID mice that had been thymectomized 1 week after birth (Tx-SCID). The severity of arthritis in these mice was assessed 3 months later. $CD4^+$ or $CD8^+$ T cells were prepared by MACS (Miltenyi Biotec) with more than 95% purity. Bone marrow cells were treated with anti-Thy-1, anti-CD4 and anti-CD8 antibody and rabbit complement before transfer[19].

T-cell-deficient athymic BALB/c nude mice (Fig. 1w), whereas transfer of the sera from the same SKG mice did not (data not shown). Transfer of thymocyte suspensions from arthritic or non-arthritic young SKG mice also elicited severe arthritis in BALB/c nude mice and T/B-cell-deficient C.B-17 severe combined immunodeficiency (SCID) mice (Fig. 1x), whereas thymocyte transfer from normal BALB/c mice did not[8]. Furthermore, transfer of T-cell-depleted bone marrow cell suspensions from SKG mice produced severe arthritis in SCID mice, but not in SCID mice thymectomized before the transfer (Fig. 1x). These results collectively indicate that, first, the RA-like arthritis in SKG mice is a genuine autoimmune disease mediated by apparently joint-specific $CD4^+$ T cells; second, the SKG thymus is continuously generating arthritogenic autoimmune T cells; and, third, the SKG bone marrow cells give rise to such arthritogenic T cells through the normal thymic environment, indicating that the arthritogenic abnormality in SKG mice is intrinsic to T cells.

The primary cause of the arthritis in SKG mice is a genetic abnormality, not vertical or horizontal transmission of arthritogenic microbes. The offspring of crosses between SKG and normal BALB/c mice, whether the mother was SKG or BALB/c, developed no arthritis (Fig. 2a). In contrast, arthritis with a clinical course and severity similar to that in SKG mice occurred in about 50% of the N_2 generation obtained by crossing the non-arthritic F_1 hybrids with SKG. Thus, the genetic abnormality was presumably of a single gene locus (designated the *skg* gene) and inherited in an autosomal recessive fashion with nearly 100% penetrance of the trait in homozygotes raised in our conventional environment.

Linkage analysis between the development of macroscopically evident arthritis and the homozygosity of chromosome-specific microsatellite markers, performed by using the N_2 generation with *Mus musculus castaneus* (CAST/Ei) (that is, SKG × (SKG × CAST/Ei)F_1 mice), mapped the *skg* locus to the centromeric portion of chromosome 1 with the lod score of the locus as infinite (Fig. 2b). Another significant linkage was with the region around the *H-2* locus on chromosome 17 (Fig. 2c). This linkage was observed only when the mice were maintained in a nearly specific-pathogen-free (SPF) condition, but not in arthritis-prone non-SPF conventional

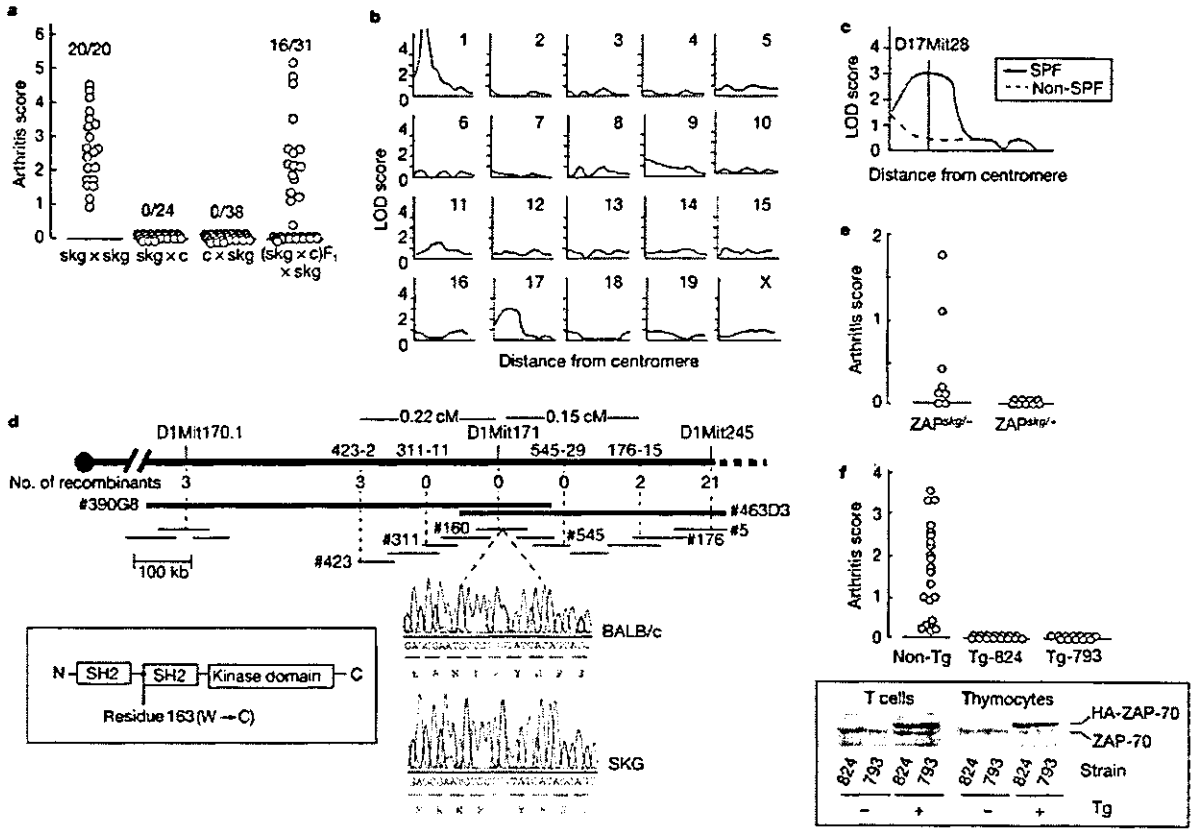

Figure 2 Genetic study of SKG arthritis. **a**, Autosomal recessive inheritance of SKG arthritis. skg × skg, F_1 of mating SKG females with SKG males; skg × c and c × skg, F_1 of mating SKG females with BALB/c males, and BALB/c females with SKG males, respectively; (skg × c)F_1 × skg, N_2 mice of backcrossing (SKG × BALB/c)F_1 mice with SKG mice. **b**, Genome-wide mapping of the *skg* locus. The LOD score curves were obtained by genotyping 58 arthritis-bearing N_2 mice by detecting microsatellite markers (Mouse MapPairs) locating every ~10 cM interval on each chromosome, in accordance with the manufacturer's instruction (Research Genetics). Chromosomes are identified with a number or X in each panel. **c**, Contribution of the loci on chromosome 17 to genetic susceptibility to SKG arthritis in a SPF condition. **d**, Genetic map of the *skg* locus on chromosome 1 with the number of recombinants and physical map of the locus with YAC and BAC clones. Inset shows the structure of the ZAP-70 protein and the position of the *skg* mutation. The ZAP-70^{W163C} mutation in SKG mice was not found in other mouse strains including C57BL/6, C3H, DBA/1, DBA/2, 129$^+$Ter/SV, FvB/N, NOD, MRL-lpr, NZW and CAST/Ei. **e**, SKG mice were mated with heterozygotes of ZAP-70-deficient mice, and the resulting ZAP-$70^{skg/-}$ or ZAP-$70^{skg/+}$ mice were assessed for joint swelling at 5 months of age. **f**, Rescue of SKG arthritis by expressing human normal ZAP-70 transgene[9]. The arthritis score of Tg-824 or Tg-793 mice, which were backcrossed three times to SKG mice, was assessed at 8 months of age. The expression of transgene-derived human ZAP-70 protein with HA-tag was assessed by western blotting with antibody against human ZAP-70 (Santa Cruz Biotech).

condition (lod scores at the D17Mit28 locus: 2.95 in SPF compared with 0.40 in non-SPF). In the former condition, homozygosity of the H-2^d haplotype conferred higher genetic susceptibility to the arthritis, indicating that a polymorphism of the major histocompatibility complex (MHC) gene or the gene(s) linked to it can contribute to determining the susceptibility depending on the environmental conditions.

To identify the *skg* gene, we then constructed a high-resolution genetic map of the *skg* region by using 1,352 mice with arthritis among a total of 2,939 N_2 mice (Fig. 2d). The mapping localized the *skg* locus to a 0.37-cM interval between two simple sequence-length polymorphism markers (nos 176-15 and 423-2), covered by two yeast artificial chromosomes (YACs) and ten bacterial artificial chromosomes (BACs) (Fig. 2d, top). Sequencing of several of these BACs localized the ZAP-70 gene on BAC no. 160. Sequencing of the entire coding region of ZAP-70 cDNA from SKG mice and comparison of the sequence with that of BALB/c mice revealed a homozygous G-to-T substitution at nucleotide 489 in the SKG ZAP-70 gene, which altered codon 163 from tryptophan to cysteine (W163C) (Fig. 2d, bottom). This nucleotide substitution existed in the genomic DNA of SKG mice but not in other strains (see legend to Fig. 2). The position of the mutation corresponds to the initial amino-acid residue of the carboxy-terminal SH2 (SH2C) domain of ZAP-70 (Fig. 2d, inset).

To confirm that the ZAP-70^{W163C} mutation was primarily responsible for SKG arthritis, we crossed SKG mice, which had a ZAP-$70^{skg/skg}$ genotype, with the heterozygotes of ZAP-70-deficient mice (ZAP-$70^{+/-}$) to produce mice with a ZAP-$70^{skg/+}$ or ZAP-$70^{skg/-}$ genotype[9] and assessed the development of arthritis in these mice (Fig. 2e). Most of the ZAP-$70^{skg/-}$ mice developed arthritis spontaneously by 3 months of age, in contrast with no arthritis in the ZAP-$70^{skg/+}$ mice. Other immunological abnormalities of T cells and thymocytes were also similar between SKG mice and ZAP-$70^{skg/-}$ mice but these were corrected in ZAP-$70^{skg/+}$ mice (Supplementary Fig. 2a, and see below). Furthermore, transgenic (Tg) expression of the normal human ZAP-70 gene in SKG mice

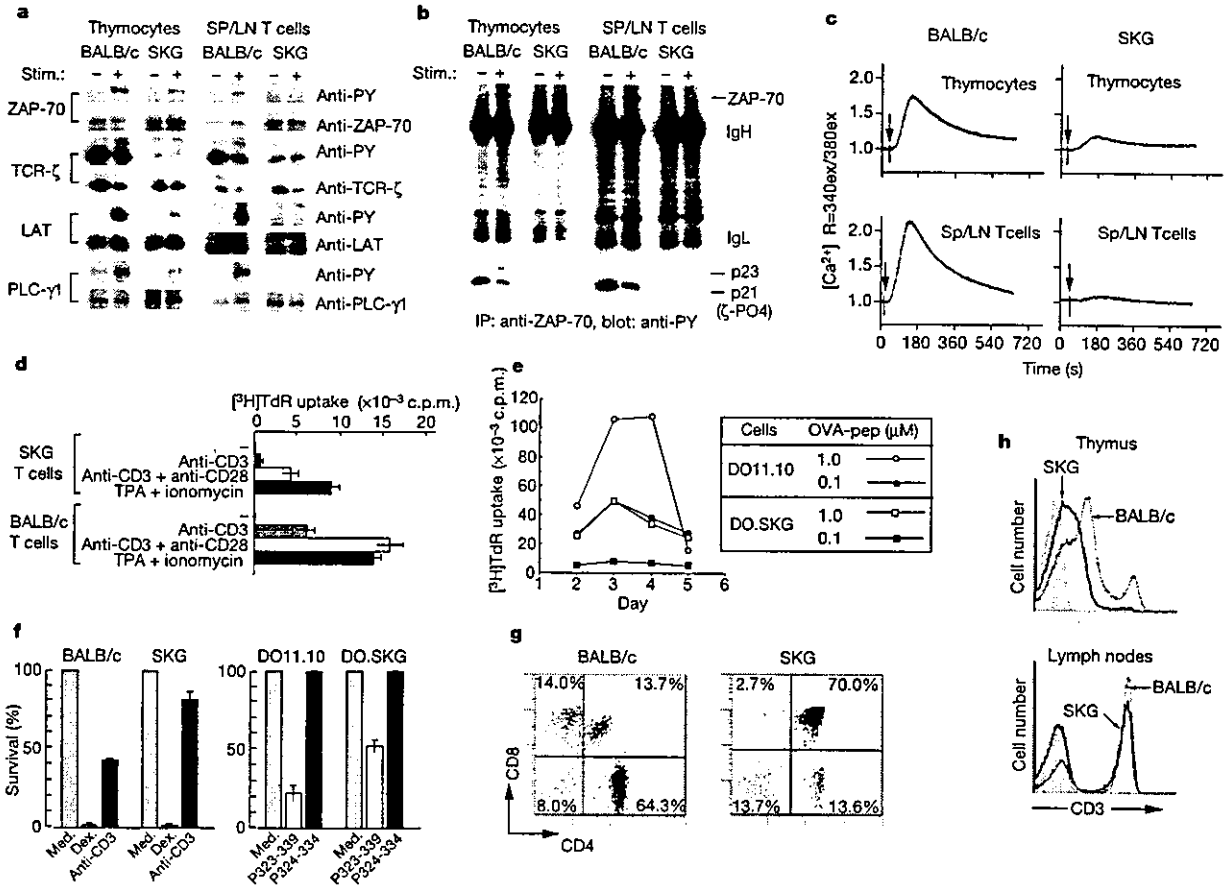

Figure 3 T-cell abnormalities in SKG mice. **a**, Impaired TCR signal transduction in SKG mice. Tyrosine phosphorylation status was assessed by immunoprecipitation and western blotting for ZAP-70, TCR-ζ, LAT and PLC-γ after anti-CD3 mAb stimulation of SKG or BALB/c thymocytes or spleen and lymph node (SP/LN) T cells. **b**, Association between ZAP-70 and TCR-ζ after CD3 crosslinking in SKG T cells and thymocytes. IP, immunoprecipitation. **c**, Ca^{2+} mobilization in SKG T cells or thymocytes after TCR stimulation. **d**, Proliferative responses of SKG T cells to various T-cell stimulations. **e**, Proliferation of $CD4^+$ T cells from DO11.10 or DO.SKG mice stimulated with the indicated concentrations of ovalbumin (OVA) peptides in the presence of BALB/c antigen-presenting cells. **f**, Apoptosis of SKG or BALB/c thymocytes cultured with medium alone (med.), anti-CD3 mAb (2C11, 1 μg ml^{-1}) or dexamethasone (Dex.) (100 nM) (left); apoptosis of DO11.10 or DO.SKG thymocytes cultured with medium alone or indicated ovalbumin peptides (1 μM) (right), as described previously[9]. **g**, Apoptosis of thymocytes in SKG or BALB/c mice injected intraperitoneally with anti-CD3 mAb (2C11; 250 μg) 3 days previously[9]. These figures represent three independent experiments. **h**, Staining of thymocytes or lymph-node cells from a 2-month-old SKG or BALB/c mouse with anti-CD3 mAb.

under the *lck* proximal promoter, which resulted in specific expression of the Tg ZAP-70 protein in thymocytes and peripheral T cells in two Tg lines, completely inhibited the development of arthritis and corrected other immunological abnormalities, contrasting with 100% incidence of arthritis in non-Tg littermates (Fig. 2f and Supplementary Fig. 2b).

Taken together, these results indicate that the ZAP-70^{W163C} alteration is not a mere polymorphism but is the causative mutation of SKG arthritis.

To determine, then, how the ZAP-70 mutation affects T-cell signal transduction, we assessed thymocytes and T cells from SKG or BALB/c mice for the tyrosine-phosphorylation status of major signal transduction molecules, including ZAP-70, TCR-ζ, LAT and PLC-γ1 (refs 6, 10–12; Fig. 3a, b). After stimulation with anti-CD3 monoclonal antibody (mAb), the levels of phosphorylation of these molecules were extremely low in SKG thymocytes and T cells. Calcium mobilization, one of the earliest events induced by TCR stimulation, was also greatly impaired in SKG thymocytes and T cells, presumably because of the decreased phosphorylation of PLC-γ1 (Fig. 3c). Immunoprecipitation of ZAP-70 from stimulated SKG thymocytes or T cells failed to co-precipitate tyrosine-phosphorylated p21 and p23 isoforms of TCR-ζ, indicating defective interactions between ZAP-70 and TCR-ζ[10,11] (Fig. 3b). Furthermore, downstream mitogen-activated protein (MAP) kinase signalling pathways involving ERK, JNK and p38 MAP kinases were also attenuated in SKG thymocytes[13] (Supplementary Fig. 3). SKG T cells showed no enhancement of the expression of Syk, another protein tyrosine kinase that might compensate for the role of ZAP-70 in T cells[14] (T.T., unpublished data). These results collectively indicate that the ZAP-70^{W163C} mutation might impair the recruitment and association of ZAP-70 to tyrosine-phosphorylated immunoreceptor tyrosine-based activation motifs (ITAMs) of TCR-ζ and CD3 chains, thereby altering signal transduction through ZAP-70.

In accord with this attenuated signal transduction through ZAP-70, SKG T cells were hyporesponsive to polyclonal TCR stimulation *in vitro*, for example with anti-CD3 mAb, whereas they responded well to stimulation by 12-*O*-tetradecanoylphorbol-13-acetate (TPA) and ionomycin, which transduces a signal to TCR-distal pathways (Fig. 3d). When the *skg* gene was homozygously introduced to DO11.10 TCR-Tg mice, in which most T cells express Tg TCRs specific for an ovalbumin peptide[15], T cells from such mice (designated DO.SKG mice) required a peptide concentration 10-fold that in DO11.10 T cells to exhibit an equivalent magnitude of proliferation (Fig. 3e). Furthermore, SKG thymocytes were resistant to apoptosis induced by TCR stimulation, but not to dexamethasone-induced apoptosis, as shown by the stimulation of SKG or DO.SKG thymocytes *in vitro* with anti-CD3 mAb or the specific peptide, respectively (Fig. 3f), or by inoculation with anti-CD3 mAb *in vivo* (Fig. 3g).

SKG mice were also aberrant in T-cell development. In comparison with normal BALB/c mice, TCR^{high} mature thymocytes decreased in number and ratio, whereas TCR^{low} immature thymocytes increased in the SKG thymus; the levels of TCR expression on

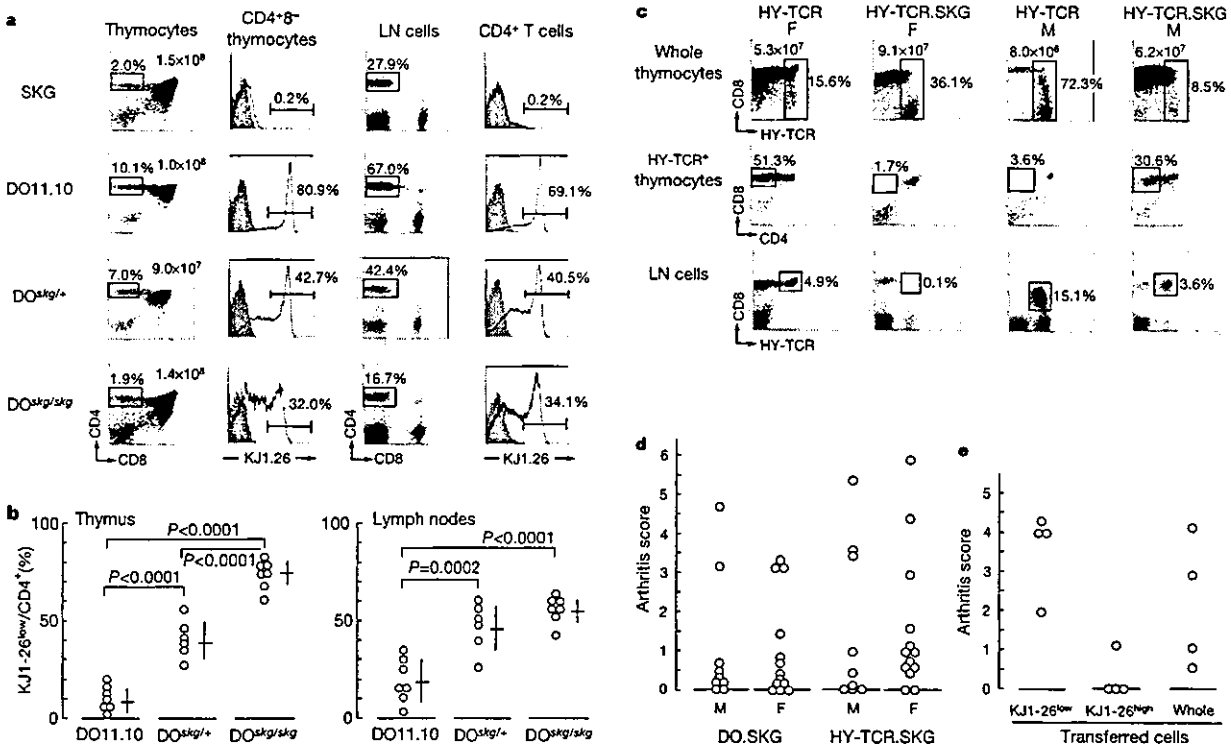

Figure 4 Altered thymic T-cell selection in SKG mice. **a**, Staining of thymocytes or lymph-node cells from a 4-month-old DO11.10, DO$^{skg/skg}$ or DO$^{skg/+}$ mouse with the indicated monoclonal antibodies. Dot-plot figures are scaled logarithmically. Ordinates of histograms denote cell number (arbitrary units). **b**, The percentage of KJ1-26^{low} T cells among CD4$^+$CD8$^-$ thymocytes or CD4$^+$ T cells was also assessed for individual DO11.10, DO$^{skg/+}$ or DO$^{skg/skg}$ mice. **c**, Staining of thymocytes or lymph-node cells from a 4-month-old female or male HY-TCR or HY-TCR.SKG transgenic mouse with the indicated monoclonal antibodies. **d**, Arthritis scores of 6-month-old DO.SKG or HY-TCR.SKG mice. **e**, Adoptive transfer of arthritis from arthritis-bearing DO.SKG mice to SCID mice, which were assessed for joint swelling 2 months later. Each fraction of cells (10^6) was purified by cell sorter from CD4$^+$ lymph node and spleen cells.

mature thymocytes or peripheral T cells were comparable between the two strains (Fig. 3h). The numbers of peripheral $CD4^+$ and $CD8^+$ T cells consequently decreased in SKG mice, with a relative increase in B cells (Supplementary Fig. 4). There was no significant difference in the total number of thymocytes or spleen cells, the thymic architecture, the number and function of natural killer cells (which express ZAP-70) or the composition of T-cell subpopulations expressing particular TCR Vα or Vβ families (Supplementary Fig. 5).

We then assessed the effects of the *skg* mutation on thymic positive and negative selection by introducing the *skg* gene homozygously into TCR-Tg mice[15,16]. In DO.SKG (that is, $DO^{skg/skg}$) mice, the number of $CD4^+CD8^-$ mature thymocytes decreased to ~20% of normal DO11.10 mice (Fig. 4a). Furthermore, only ~30% of $CD4^+CD8^-$ thymocytes were Tg-TCR^{high} (when stained with clonotype-specific KJ1-26 mAb)[15] in contrast to ~80% in DO11.10 mice (Fig. 4a, b); the rest of $CD4^+CD8^-$ thymocytes (that is, KJ1-26^{low}, hence Tg-TCR^{low} thymocytes) in $DO^{skg/skg}$ mice seemed to express endogenous TCR α-chains. Similarly, Tg-TCR^{high} T cells constituted only ~30% of $CD4^+$ T cells in the periphery of $DO^{skg/skg}$ mice, contrasting with ~70% in DO11.10 mice (Fig. 4a, b); Tg-TCR^{low} T cells in $DO^{skg/skg}$ mice expressed endogenous α-chains associated with transgenic β-chains (Supplementary Fig. 6). In *skg*-heterozygous $DO^{skg/+}$ mice, the decrease or increase in the percentage of Tg-TCR^{high} or Tg-TCR^{low} T cells, respectively, in the thymus and the periphery was intermediate between that in the $DO^{skg/skg}$ and that in DO11.10 mice (Fig. 4a, b).

In HY-TCR Tg mice that express transgenic TCRs specific for male-specific HY antigens on an $H\text{-}2^b$ background, female HY-TCR Tg mice positively selected HY-$TCR^+CD8^+CD4^-$ thymocytes (detected by clonotype-specific T3.70 mAb)[16]. In contrast, female HY-TCR Tg mice with the homozygous *skg* gene (designated HY-TCR.SKG Tg mice) on an $H\text{-}2^b$ background hardly showed any positive selection of HY-$TCR^+CD8^+CD4^-$ thymocytes and T cells[17] (Fig. 4c). However, in contrast to substantial deletion of HY-$TCR^+CD8^+CD4^-$ thymocytes in male HY-TCR Tg mice, male HY-TCR.SKG Tg mice showed efficient positive selection of HY-$TCR^+CD8^+CD4^-$ thymocytes in almost a comparable number to those in female HY-TCR Tg mice. Furthermore, HY-TCR^+ peripheral T cells in male HY-TCR.SKG Tg mice expressed nearly normal levels of CD8 expression, contrasting with low-level CD8 expression in male HY-TCR Tg mice[16].

Both DO.SKG and HY-TCR.SKG mice developed arthritis at high incidences (Fig. 4d). Transfer of Tg-TCR^{low} cells (as KJ1-26^{low} cells) from such arthritis-bearing DO.SKG mice to C.B-17 SCID mice induced arthritis, whereas transfer of Tg-TCR^{high} cells did not (Fig. 4e), indicating that TCR-Tg mice with the *skg* mutation positively select arthritogenic T cells expressing endogenous TCR α-chains paired with transgenic β-chains (see above).

Taken together, these results show that the *skg* mutation alters the sensitivity of developing thymocytes to both positive and negative selection, thereby leading to positive selection of otherwise negatively selected autoimmune T cells. This recessive mutation affects T-cell selection even in the heterozygotes, although to a smaller degree than in the homozygotes. Furthermore, the degree of impairment in T-cell signal transduction through ZAP-70 can determine the degree of thymic positive or negative selection, and consequently the phenotype of immunological diseases. The *skg* mutation of the SH2C domain of ZAP-70 elicits autoimmune arthritis, whereas a mutation in the kinase domain of ZAP-70 leads to a severe impairment of positive selection and hence total T-cell deficiency[18].

On the assumption that thymic positive and negative selection of developing T cells requires a certain range of TCR signal through ZAP-70, the *skg* mutation is likely to raise the threshold of TCR avidity for self-peptide/MHC ligands required for the selection to compensate for the reduced signal through the aberrant ZAP-70. This results in a 'selection shift' of the T-cell repertoire towards high reactivity to self-peptide/MHC ligands in the thymus, leading to the thymic production of highly self-reactive T cells that would not be produced by the normal thymuses of ZAP-70-intact animals. The pathogenic self-reactive T cells thus produced by the SKG thymus apparently overcome the mechanisms of peripheral self-tolerance, for example, mediated by naturally occurring $CD25^+CD4^+$ regulatory T cells[8,19]. However, it remains to be determined whether the *skg* mutation might also alter the repertoire of $CD25^+CD4^+$ regulatory T cells or somehow affect their suppressive activity[8,19].

A critical question on SKG arthritis is why this general alteration in T-cell repertoire should lead to the predominant development of autoimmune arthritis but not other autoimmune diseases. In contrast with other organ-specific autoimmune diseases in which self-reactive T cells destroy the target cells (for example, type 1 diabetes due to destruction of insulin-secreting pancreatic β-cells), a cardinal feature of autoimmune arthritis in SKG mice (and also RA in humans) is that self-reactive T cells do not destroy synoviocytes but stimulate them to proliferate[1–3]. This is partly due to a high sensitivity of synoviocytes to various stimuli that can activate them (as also illustrated by other arthritis models[7,19–25]) and their distinct capacity to secrete proinflammatory cytokines (such as interleukin-1, interleukin-6 and tumour necrosis factor-α) and chemical mediators that destroy the surrounding cartilage and bone[1–3,26,27]. It is therefore likely that this unique combination of a high and broad self-reactivity of SKG T cells and a high susceptibility of synovial cells to inflammatory stimuli (including T-cell self-reactivity) leads to predominant development of autoimmune arthritis in SKG mice.

Our findings indicate that mutations of other loci of the ZAP-70 gene or the genes encoding other signalling molecules especially at TCR proximal steps, even if they are heterozygous mutations, might contribute to the development of autoimmune disease by affecting thymic T-cell selection[28–30]. Indeed, we have recently found heterozygous mutations in the ITAM regions of the TCR-ζ chain gene in 2.5% of 160 RA patients in our hospital (H.H., N.S., S.N., T.N. and S.S., unpublished observations). Physical association between these mutated TCR-ζ chain molecules and the normal ZAP-70 molecules, assessed by surface plasmon resonance, was significantly lower than normal as observed between the mutated ZAP-70 in SKG mice and the normal TCR-ζ chain (T.N. and S.S., unpublished data). As RA is a heterogeneous disease with complex genetics[1–3], RA with a similar aetiology to SKG arthritis represents only a fraction of the disease. Nevertheless, further analyses of SKG arthritis at each step of the pathogenetic pathway from the ZAP-70 mutation, through thymic generation of autoimmune T cells, to the activation of arthritogenic T cells and inflammatory destruction of the joint, will explain how genetic and environmental factors contribute to the development of RA. This will help in the design of effective methods of detection, treatment and prevention of RA. □

Methods

Scoring of joint swelling

Joint swelling was monitored by inspection and scored as follows: 0, no joint swelling; 0.1, swelling of one finger joint; 0.5, mild swelling of wrist or ankle; 1.0, severe swelling of wrist or ankle. Scores for all fingers of forepaws and hindpaws, wrists and ankles were totalled for each mouse.

Enzyme-linked immunosorbent assay (ELISA)

Affinity-purified mouse IgG (5 μg ml^{-1}), 10 μg ml^{-1} bovine type II collagen (Funakoshi), 5 μg ml^{-1} double or single-stranded-DNA, or 10 μg ml^{-1} HSP-70 of *Mycobacterium tuberculosis* in PBS, pH 7.2, were used for overnight coating of ELISA plates (Flow Laboratories)[7,8]. Test sera were diluted 1:10 for anti-type II collagen or anti-HSP-70 assay, 1:20 for RF assay, or 1:40 for anti-DNA assay. Alkaline-phosphatase-conjugated anti-mouse IgG or IgM (for RF assay) (Southern Biotechnology Associates) was used at 1 μg ml^{-1} as the secondary reagent[7,8]. Pooled serum from MRL-lpr mice was used as the standard of arbitrary units in the RF, anti-DNA or anti-HSP70 antibody assay[7]. The titre of anti-CII antibody was expressed as attenuance. The amount of immune complex was measured by anti-C3 assay; the serum concentration of IgG was measured by the single radial immunodiffusion method[7].

In vitro T-cell activation

SKG or BALB/c T cells (3.0×10^4) were stimulated for 72 h with plate-bound anti-CD3 mAb (2C11) in the presence or absence of plate-bound anti-CD28 mAb in RPMI-1640 medium supplemented with 10% fetal calf serum and 50 μM 2-mercaptoethanol. Cells were also stimulated with TPA (1.4 ng ml^{-1}) and ionomycin (0.14 μM). KJ1.26$^+$ T cells from DO or DO.SKG mice were stimulated with ovalbumin (323–339) peptide in the presence of X-irradiated syngeneic spleen cells (10^5 cells) as antigen-presenting cells in 96-well round-bottomed plates. The incorporation of [^{3}H]thymidine by proliferating lymphocytes during the last 6 h of the culture was measured.

Immunoprecipitation and western blotting

Thymocytes or purified T cells (5×10^6) were incubated with anti-CD3 mAb (2C11) for 20 min, followed by cross-linking with antibody against Armenian hamster immunoglobulin (Jackson ImmunoResearch) (10 μg ml^{-1}) at 37 °C for the indicated duration. For immunoprecipitation, cells were lysed with RIPA buffer (0.5% Triton X-100, 20 mM Tris-HCl pH 7.5, 1 mM EDTA, 150 mM NaCl, 20 mM NaF, 1 mM Na_3VO_4) supplemented with protease inhibitors. The immune complexes were recovered by Protein A-conjugated Sepharose beads. For western blot analyses, cells were directly lysed by sample-loading buffer for SDS–polyacrylamide gel electrophoresis (SDS–PAGE) and immediately boiled for 4 min. Recovered immune complexes or total cell lysates were subjected to SDS–PAGE and transferred to poly(vinylidene difluoride) membranes, which were blotted with various antibodies after being blocked with PBS/5% BSA. Antibodies specific for the following proteins were used: ZAP-70 (Santa Cruz Biotech), TCR-ζ (Santa Cruz Biotech), LAT (Upstate Biotechnology), PLC-γ1 (Upstate Biotechnology), activated or total ERK1/2, SAPK/JNK and p38 MAP kinases (Cell Signalling Technology) or phosophotyrosine (4G10) (Upstate Biotechnology).

Calcium mobilization

Thymocytes or purified T cells were loaded with Fura-2 acetoxymethyl ester (Nacarai) for 30 min at 37 °C. Cells were then incubated with anti-CD3 mAb as described above, washed and resuspended with PBS. $CaCl_2$ was added to the samples 2 min before cross-linking cell surface-bound anti-CD3 mAb with anti-hamster antibody (Jackson ImmunoResearch). Fura-2 fluorescence was measured by a spectrofluorimeter (Nihon Bunkou).

Received 4 August; accepted 13 October 2003; doi:10.1038/nature02119.

1. Harris, E. D. *Rheumatoid Arthritis* (W. B. Saunders, Philadelphia, 1997).
2. Feldmann, M., Brennan, F. M. & Maini, R. N. Rheumatoid arthritis. *Cell* 85, 307–310 (1996).
3. Firestein, G. F. in *Textbook of Rheumatology* 5th edn (eds Kelley, W. N., Ruddy, S., Harris, E. D. & Sledge, C. B.) 851–897 (W. B. Saunders, Philadelphia, 1997).
4. Marrack, P., Kappler, J. & Kotzin, B. L. Autoimmune disease: why and where it occurs. *Nature Med.* 7, 899–905 (2001).
5. von Boehmer, H. *et al.* Thymic selection revisited: how essential is it? *Immunol. Rev.* 191, 62–78 (2003).
6. Chan, A. C., Iwashima, M., Turck, C. W. & Weiss, A. ZAP-70: a 70 kd protein-tyrosine kinase that associates with the TCR zeta chain. *Cell* 71, 649–662 (1992).
7. Sakaguchi, S. & Sakaguchi, N. Thymus and autoimmunity: capacity of the normal thymus to produce pathogenic self-reactive T cells and conditions required for their induction of autoimmune disease. *J. Exp. Med.* 172, 537–545 (1990).
8. Itoh, M. *et al.* Thymus and autoimmunity: production of CD25$^+$ CD4$^+$ naturally anergic and suppressive T cells as a key function of the thymus in maintaining immunologic self-tolerance. *J. Immunol.* 162, 5317–5326 (1999).
9. Negishi, I. *et al.* Essential role for ZAP-70 in both positive and negative selection of thymocytes. *Nature* 376, 435–438 (1995).
10. van Oers, N. S. *et al.* The 21- and 23-kD forms of TCR zeta are generated by specific ITAM phosphorylations. *Nature Immunol.* 1, 322–328 (2000).
11. Iwashima, M. *et al.* Sequential interactions of the TCR with two distinct cytoplasmic tyrosine kinases. *Science* 263, 1136–1139 (1994).
12. Zhang, W., Sloan-Lancaster, J., Kitchen, J., Trible, R. P. & Samelson, L. E. LAT: the ZAP-70 tyrosine kinase substrate that links T cell receptor to cellular activation. *Cell* 92, 83–92 (1998).
13. Rincon, M. MAP-kinase signaling pathway in T cells. *Curr. Opin. Immunol.* 13, 339–345 (2001).
14. Noraz, N. *et al.* Alternative antigen receptor (TCR) signaling in T cells derived from ZAP-70-deficient patients expressing high levels of Syk. *J. Biol. Chem.* 275, 15832–15838 (2000).
15. Murphy, K. M., Heimberger, A. B. & Loh, D. Y. Induction by antigen of intrathymic apoptosis of CD4$^+$CD8$^+$TCR^{lo} thymocytes *in vivo*. *Science* 250, 1720–1723 (1990).
16. Kisielow, P., Bluthmann, H., Staerz, U. D., Steinmetz, M. & von Boehmer, H. Tolerance in T-cell-receptor transgenic mice involves deletion of nonmature CD4$^+$8$^+$ thymocytes. *Nature* 333, 742–746 (1988).
17. Kisielow, P., Teh, H. S., Bluthmann, H. & von Boehmer, H. Positive selection of antigen-specific T cells in thymus by restricting MHC molecules. *Nature* 335, 730–733 (1988).
18. Wiest, D. L. *et al.* A spontaneously arising mutation in the DLAARN motif of murine ZAP-70 abrogates kinase activity and arrests thymocyte development. *Immunity* 6, 663–671 (1997).
19. Sakaguchi, S., Sakaguchi, N., Asano, M., Itoh, M. & Toda, M. Immunologic self-tolerance maintained by activated T cells expressing IL-2 receptor α-chains (CD25). Breakdown of a single mechanism of self-tolerance causes various autoimmune diseases. *J. Immunol.* 155, 1151–1164 (1995).
20. Keffer, J. *et al.* Transgenic mice expressing human tumor necrosis factor: a predictive genetic model of arthritis. *EMBO J.* 10, 4025–4031 (1991).
21. Kouskoff, V. *et al.* Organ-specific disease provoked by systemic autoimmunity. *Cell* 87, 811–822 (1996).
22. Pals, S. T., Radaszkiewicz, T., Roozendaal, L. & Gleichman, E. Chronic progressive polyarthritis and other symptoms of collagen vascular disease induced by graft-versus-host reaction. *J. Immunol.* 134, 1475–1482 (1985).
23. Nishimura, H., Nose, M., Hiai, H., Minato, N. & Honjo, T. Development of lupus-like autoimmune diseases by disruption of the PD-1 gene encoding an ITIM motif-carrying immunoreceptor. *Immunity* 11, 141–151 (1999).
24. Horai, R. *et al.* Development of chronic inflammatory arthropathy resembling rheumatoid arthritis in interleukin 1 receptor antagonist-deficient mice. *J. Exp. Med.* 191, 313–320 (2000).
25. Atsumi, T. *et al.* A point mutation of Tyr-759 in interleukin 6 family cytokine receptor subunit gp130 causes autoimmune arthritis. *J. Exp. Med.* 196, 979–990 (2002).
26. Dayer, J. M. & Burger, D. Cytokines and direct cell contact in synovitis: relevance to therapeutic intervention. *Arthritis Res.* 1, 17–20 (1999).
27. Naka, T., Nishimoto, N. & Kishimoto, T. The paradigm of IL-6: from basic science to medicine. *Arthritis Res.* 4 (Suppl. 3), S233–S242 (2002).
28. Werlen, G., Hausmann, B., Naeher, D. & Palmer, E. Signaling life and death in the thymus: timing is everything. *Science* 299, 1859–1863 (2003).
29. Nambiar, M. P. *et al.* T cell signalling abnormalities in systemic lupus erythematosus are associated with increased mutations/polymorphisms and splice variants of T cell receptor zeta chain messenger RNA. *Arthritis Rheum.* 44, 1336–1350 (2001).
30. Takeuchi, T. *et al.* TCR zeta chain lacking exon 7 in two patients with systemic lupus erythematosus. *Int. Immunol.* 10, 911–921 (1998).

Supplementary Information accompanies the paper on **www.nature.com/nature.**

Acknowledgements We thank H. von Boemer for transgenic mice; M. Singh (GBF, Germany) for a gift of recombinant HSP-70 through the support of the UNDP/World Bank/WHO Special Program for Research and Training on Tropical Diseases; F. Melchers, R. Zinkernagel, K. Yamamoto, R. Suzuki and Z. Fehervari for discussion; A. Kosugi and T. Nakayama for reagents; and E. Moriizumi for immunohistochemistry and histology. This work was supported by grants-in-aid from the Ministry of Education, Science, Sports and Culture, the Ministry of Human Welfare, Japan Science and Technology Corporation, and the Organization for Pharmaceutical Safety and Research of Japan.

Authors' contributions The SKG strain was established by S.S. and N.S. The experiments in Figs 1, 2a–d, 3f–h, 4, Supplementary Figs 1, 4 and 6 were conducted by N.S. and S.S.; those in Fig. 2b–d by Ta.T., N.S., H.H., To.T., S.Y., T. S., S.N. and S.S.; those in Figs 2e, f, 3a–c, e and Supplementary Fig. 2 by Ta.T.; that in Fig. 3d by To.T.; that in Supplementary Fig. 3 by T.N., and that in Supplementary Fig. 5 by T.M. ZAP-70-deficient mice were provided by I.N.

Competing interests statement The authors declare that they have no competing financial interests.

Correspondence and requests for materials should be addressed to S.S. (shimon@frontier.kyoto-u.ac.jp).

A positive-feedback-based bistable 'memory module' that governs a cell fate decision

Wen Xiong & James E. Ferrell Jr

Department of Molecular Pharmacology, Stanford University School of Medicine, Stanford, California 94305-5174, USA

The maturation of *Xenopus* oocytes can be thought of as a process of cell fate induction, with the immature oocyte representing the default fate and the mature oocyte representing the induced fate[1,2]. Crucial mediators of *Xenopus* oocyte maturation, including the p42 mitogen-activated protein kinase (MAPK) and the cell-division cycle protein kinase Cdc2, are known to be organized into positive feedback loops[3]. In principle, such positive feedback loops could produce an actively maintained 'memory' of a transient inductive stimulus and could explain the irreversibility of maturation[3–6]. Here we show that the p42 MAPK and Cdc2 system normally generates an irreversible biochemical response from a transient stimulus, but the response becomes transient when positive feedback is blocked. Our results explain how a group of intrinsically reversible signal transducers can generate an irreversible response at a systems level, and show how a cell fate can be maintained by a self-sustaining pattern of protein kinase activation.

Immature *Xenopus* oocytes are arrested in a G2-like phase of the cell cycle. In response to steroid hormones, the oocyte is released

International weekly journal of science

nature

Costimulatory signals mediated by the ITAM motif cooperate with RANKL for bone homeostasis

Takako Koga[*1,2], Masanori Inui[*3], Kazuya Inoue[*3], Sunhwa Kim[*1], Ayako Suematsu[*1,2], Eiji Kobayashi[*3], Toshio Iwata[*3], Hiroshi Ohnishi[*4], Takashi Matozaki[*4], Tatsuhiko Kodama[*5], Tadatsugu Taniguchi[*1], Hiroshi Takayanagi[*1,2] & Toshiyuki Takai[*3]

[*1]*Department of Immunology, Graduate School of Medicine and Faculty of Medicine, University of Tokyo, Hongo 7-3-1, Bunkyo-ku, Tokyo 113-0033, Japan*
[*2]*Department of Cellular Physiological Chemistry, Graduate School, Tokyo Medical and Dental University, and COE Program for Frontier Research on Molecular Destruction and Reconstruction of Tooth and Bone, Yushima 1-5-45, Bunkyo-ku, Tokyo 113-8549, Japan and PRESTO, Japan Science and Technology Agency (JST), Honcho 4-1-8, Kawaguchi, Saitama 332-0012, Japan*
[*3]*Department of Experimental Immunology, Institute of Development, Aging and Cancer, Tohoku University, Seiryo 4-1, Aoba-ku, Sendai 980-8575, Japan and CREST, JST, Honcho 4-1-8, Kawaguchi, Saitama 332-0012, Japan*
[*4]*Biosignal Research Center, Institute for Molecular and Cellular Regulation, Gunma University, Showa-machi 3-39-15, Maebashi 371-8512, Japan*
[*5]*Department of Molecular Biology and Medicine, Research Center for Advanced Science and Technology, University of Tokyo, Komaba 4-6-1, Meguro-ku, Tokyo 153-8904, Japan*

Reprinted from Nature, Vol. 428, No. 6984, pp. 758-763, 15 April 2004

Costimulatory signals mediated by the ITAM motif cooperate with RANKL for bone homeostasis

Takako Koga[1,2*], Masanori Inui[3*], Kazuya Inoue[3], Sunhwa Kim[1], Ayako Suematsu[1,2], Eiji Kobayashi[3], Toshio Iwata[3], Hiroshi Ohnishi[4], Takashi Matozaki[4], Tatsuhiko Kodama[5], Tadatsugu Taniguchi[1], Hiroshi Takayanagi[1,2] & Toshiyuki Takai[3]

[1]*Department of Immunology, Graduate School of Medicine and Faculty of Medicine, University of Tokyo, Hongo 7-3-1, Bunkyo-ku, Tokyo 113-0033, Japan*
[2]*Department of Cellular Physiological Chemistry, Graduate School, Tokyo Medical and Dental University, and COE Program for Frontier Research on Molecular Destruction and Reconstruction of Tooth and Bone, Yushima 1-5-45, Bunkyo-ku, Tokyo 113-8549, Japan and PRESTO, Japan Science and Technology Agency (JST), Honcho 4-1-8, Kawaguchi, Saitama 332-0012, Japan*
[3]*Department of Experimental Immunology, Institute of Development, Aging and Cancer, Tohoku University, Seiryo 4-1, Aoba-ku, Sendai 980-8575, Japan and CREST, JST, Honcho 4-1-8, Kawaguchi, Saitama 332-0012, Japan*
[4]*Biosignal Research Center, Institute for Molecular and Cellular Regulation, Gunma University, Showa-machi 3-39-15, Maebashi 371-8512, Japan*
[5]*Department of Molecular Biology and Medicine, Research Center for Advanced Science and Technology, University of Tokyo, Komaba 4-6-1, Meguro-ku, Tokyo 153-8904, Japan*

*These authors contributed equally to this work

Costimulatory signals are required for activation of immune cells[1], but it is not known whether they contribute to other biological systems. The development and homeostasis of the skeletal system depend on the balance between bone formation and resorption[2,3]. Receptor activator of NF-κB ligand (RANKL) regulates the differentiation of bone-resorbing cells, osteoclasts, in the presence of macrophage-colony stimulating factor (M-CSF)[4,5]. But it remains unclear how RANKL activates the calcium signals that lead to induction of nuclear factor of activated T cells c1, a key transcription factor for osteoclastogenesis[6]. Here we show that mice lacking immunoreceptor tyrosine-based activation motif (ITAM)[7]-harbouring adaptors[8–10], Fc receptor common γ subunit (FcRγ) and DNAX-activating protein (DAP)12, exhibit severe osteopetrosis owing to impaired osteoclast differentiation. In osteoclast precursor cells, FcRγ and DAP12 associate with multiple immunoreceptors[11–15] and activate calcium signalling through phospholipase Cγ. Thus, ITAM-dependent costimulatory signals activated by multiple immunoreceptors are essential for the maintenance of bone homeostasis. These results reveal that RANKL and M-CSF are not sufficient to activate the signals required for osteoclastogenesis.

Osteoclast differentiation induced by RANKL and M-CSF is severely blocked in the bone marrow monocyte/macrophage lineage cells (BMMs) derived from mice lacking DAP12 (ref. 16), also known as KARAP or TYROBP[9,10]. DAP12 is a membrane adaptor molecule that contains an ITAM motif, which activates calcium signalling in immune cells. Despite this *in vitro* blockage, DAP12-deficient (*DAP12*$^{-/-}$) mice exhibit only mild osteopetrosis and contain a normal number of osteoclasts. This suggests that the DAP12-mediated signal plays a crucial role in the RANKL/M-CSF-induced osteoclast formation system but that another molecule(s) can rescue the DAP12 deficiency *in vivo*[16].

To investigate the molecular basis of this discrepancy, we stimulated BMMs with RANKL and M-CSF after strictly depleting the stromal/osteoblastic cells[17]. In this osteoblast-free system, osteoclast differentiation is completely abrogated in *DAP12*$^{-/-}$ BMMs (Fig. 1a); we observed no formation of multinucleated cells

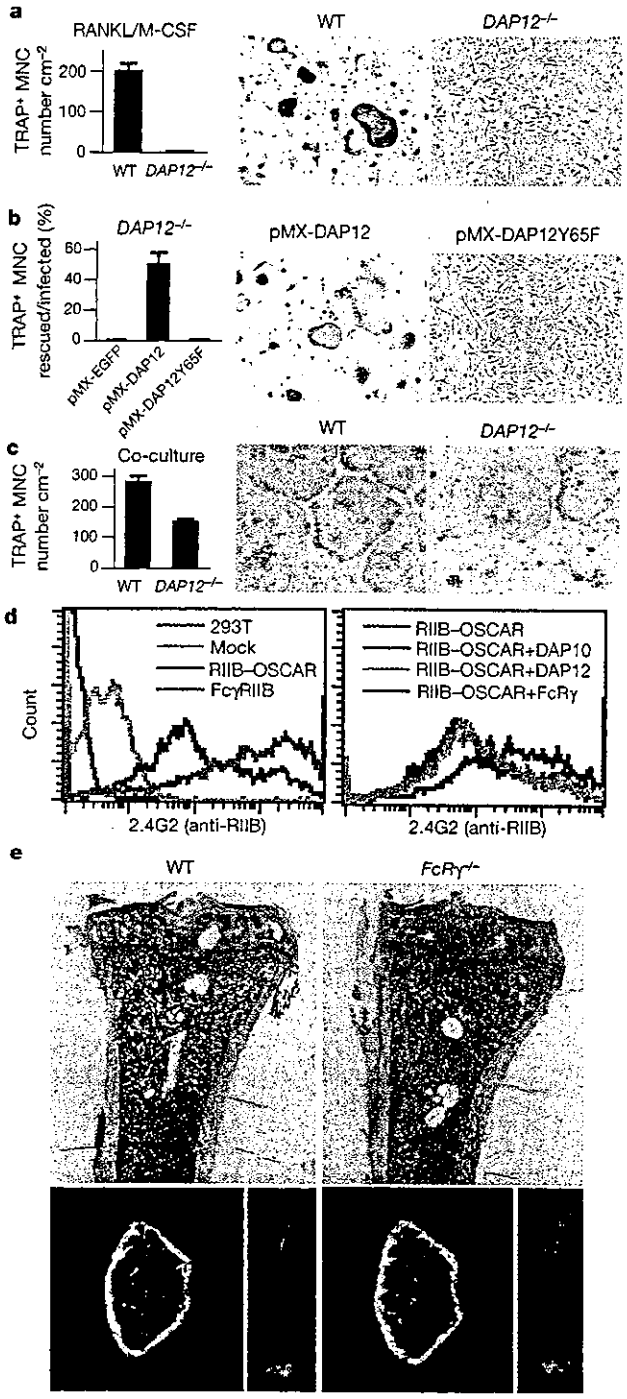

Figure 1 Impaired osteoclastogenesis in the absence of DAP12 and the compensatory mechanism by osteoblasts. **a**, Complete lack of osteoclastogenesis in *DAP12*$^{-/-}$ BMMs stimulated with RANKL/M-CSF. **b**, Rescue of osteoclastogenesis by retrovirus-mediated expression of DAP12, but not DAP12Y65F, in *DAP12*$^{-/-}$ BMMs. These multinucleated cells have a bone-resorbing activity (not shown). **c**, Osteoclast formation from *DAP12*$^{-/-}$ BMMs in co-culture with osteoblasts. Bone-resorbing activity was examined on dentine slices (not shown). **d**, Flow-cytometric analysis of cell-surface expression of FcγRIIB after overexpression of the chimaeric receptor of RIIB–OSCAR or FcγRIIB (left). Weak expression of FcγRIIB is detected by transfection of RIIB–OSCAR alone (pink line, left and right panels), but cotransfection with FcRγ exclusively increased this expression (violet line, right). **e**, Histology of tibia (upper, toluidine blue staining) and microradiographic analysis of femur (lower, microcomputed tomography, left; microradiograph, right) of *FcRγ*$^{-/-}$ mice. There was no significant abnormality.

(MNCs) positive for the marker enzyme of osteoclasts, tartrate-resistant acid phosphatase (TRAP). This differentiation block is efficiently rescued by retroviral expression of DAP12, but not by DAP12Y65F, a DAP12 mutant that does not transmit the ITAM signal[18] (Fig. 1b), indicating that the DAP12-mediated ITAM signal is required for osteoclastogenesis in this system. Interestingly, *DAP12*$^{-/-}$ BMMs undergo osteoclast differentiation in co-culture with osteoblasts[19] (Fig. 1c), showing that osteoblasts can stimulate the signal that compensates for the loss of the DAP12-mediated ITAM signal. This compensatory mechanism may explain the normal osteoclast differentiation in *DAP12*$^{-/-}$ mice *in vivo* (see Supplementary Fig. 1a, b).

The osteoclast-associated receptor (OSCAR) is an activating-type immunoglobulin-like receptor induced in RANKL-stimulated BMMs[11]. Expression of a putative OSCAR ligand in osteoblasts[11] led us to investigate OSCAR as a candidate receptor that compensates for the loss of DAP12-mediated signalling. To explore the adaptor molecules with which OSCAR associates, we constructed a chimaeric receptor composed of the extracellular portion of type IIB FcR for IgG (FcγRIIB) and the transmembrane and cytoplasmic portion of OSCAR (RIIB–OSCAR). Flow-cytometric analysis revealed that RIIB–OSCAR expression was significantly enhanced only when it was cotransfected with FcRγ (Fig. 1d). Thus, RIIB–OSCAR preferentially associates with FcRγ, another adaptor protein containing an ITAM motif, but not with DAP12 or DAP10. Immunoprecipitation analysis also verified the exclusive association of RIIB–OSCAR with FcRγ (Supplementary Fig. 1c).

The results prompted us to investigate the bone phenotype of mice deficient in FcRγ (*FcRγ*$^{-/-}$ mice)[20], but there was no significant difference in the osteoclast number and the trabecular bone volume between wild-type and *FcRγ*$^{-/-}$ mice (Fig. 1e and Supplementary Fig. 1d). In addition, there was little, if any, difference between wild-type and *FcRγ*$^{-/-}$ mice in the differentiation of osteoclasts in the RANKL/M-CSF system (Supplementary Fig. 1e) and the co-culture system (data not shown). Although OSCAR–Fc, a fusion protein of OSCAR ectodomain and Fc portion of IgG, suppresses osteoclastogenesis *in vitro*[11], our results suggest that FcRγ-mediated signals can be compensated for by other signals *in vivo*.

Considering the possibility that DAP12 and FcRγ functionally compensate for each other[21], we generated mice lacking both molecules (*DAP12*$^{-/-}$ *FcRγ*$^{-/-}$ mice). These mice exhibit severe osteopetrosis, with bone marrow filled with unresorbed bone (Fig. 2a). *DAP12*$^{-/-}$ mice show mild osteopetrosis due to impaired osteoclast activity[16], but the osteopetrosis in *DAP12*$^{-/-}$ *FcRγ*$^{-/-}$ mice is much more severe, as seen in microradiographs (Fig. 2a) and trabecular bone volume (Fig. 2b). Importantly, we observed few osteoclasts in *DAP12*$^{-/-}$ *FcRγ*$^{-/-}$ mice, indicating that the osteopetrosis is caused by defective differentiation rather than by defective activity of osteoclasts (Fig. 2c, e). Bone-morphometric analysis revealed that osteoblastic bone formation also decreases (Fig. 2d and Supplementary Fig. 2a). Thus, the ITAM-harbouring adaptors FcRγ and DAP12 are essential for osteoclast differentiation *in vivo*. Despite the severe osteopetrosis in *DAP12*$^{-/-}$ *FcRγ*$^{-/-}$ mice, these mice have no defect in tooth eruption (data not shown). In addition, we observed a very small number of TRAP^{+} MNCs in limited areas just below the epiphyseal plate (Fig. 2e and Supplementary Fig. 2b), suggesting that another adaptor molecule(s) may compensate for the function under specific conditions. In the culture system, *DAP12*$^{-/-}$ *FcRγ*$^{-/-}$ osteoclast precursor cells cannot undergo osteoclast differentiation in response to RANKL and M-CSF (Fig. 3a). Retroviral transfer of *DAP12*, but not *DAP12Y65F* or *FcRγ*, into *DAP12*$^{-/-}$ *FcRγ*$^{-/-}$ cells efficiently rescued osteoclast differentiation induced by RANKL and M-CSF. In addition, *DAP12*$^{-/-}$ *FcRγ*$^{-/-}$ precursor cells barely differentiate

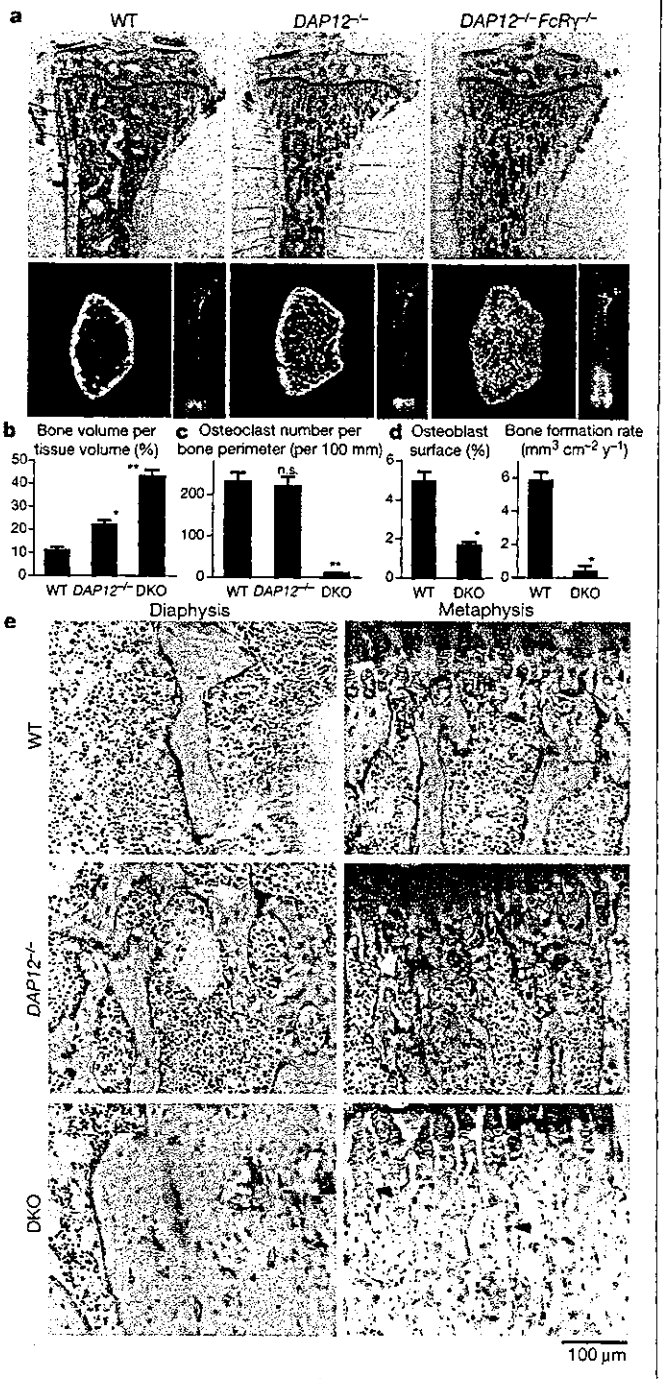

Figure 2 Severe osteopetrosis in *DAP12*$^{-/-}$ *FcRγ*$^{-/-}$ (DKO) mice due to impaired osteoclast differentiation. **a**, Histology of tibia and microradiographic analysis of femur of *DAP12*$^{-/-}$ and *DAP12*$^{-/-}$ *FcRγ*$^{-/-}$ mice (12 weeks of age). Bone-marrow cavity is absent in *DAP12*$^{-/-}$ *FcRγ*$^{-/-}$ mice. Higher radiopacity shows that *DAP12*$^{-/-}$ *FcRγ*$^{-/-}$ mice have a much more severe osteopetrotic phenotype than *DAP12*$^{-/-}$ mice. **b**, Increased trabecular bone volume in *DAP12*$^{-/-}$ *FcRγ*$^{-/-}$ mice. **c**, The number of osteoclasts is not altered in *DAP12*$^{-/-}$ mice, but is markedly decreased in *DAP12*$^{-/-}$ *FcRγ*$^{-/-}$ mice. **d**, Osteoblastic parameters in the bone-morphometric analysis of the tibia of wild-type and *DAP12*$^{-/-}$ *FcRγ*$^{-/-}$ mice (12 weeks of age). **e**, Histology of the tibia of *DAP12*$^{-/-}$ and *DAP12*$^{-/-}$ *FcRγ*$^{-/-}$ mice (TRAP and toluidine blue staining). Bone-marrow cavity is filled with unresorbed bone in the diaphysis of *DAP12*$^{-/-}$ *FcRγ*$^{-/-}$ mice. No osteoclasts are observed in the diaphysis of *DAP12*$^{-/-}$ *FcRγ*$^{-/-}$ mice, whereas the osteoclast number is normal in *DAP12*$^{-/-}$ mice. Typical sites of cartilage remnant are indicated by asterisks. In the metaphyseal area, a small number of osteoclasts are observed below epiphyseal plates in *DAP12*$^{-/-}$ *FcRγ*$^{-/-}$ mice (arrowheads).

into osteoclasts even when co-cultured with osteoblasts (Fig. 3b). In the co-culture system, retroviral transfer of *FcRγ*, but not ITAM-deficient *FcRγY65F*, also rescued osteoclast differentiation, albeit partially. These results suggest that the ITAM signal mediated through FcRγ and DAP12 is indispensable for RANKL-induced osteoclastogenesis and that each adaptor-mediated signal is differentially regulated.

FcRγ or DAP12 associates with several specific immunoreceptors for cell activation in myeloid lineage cells[13,21,22]. To identify receptors that associate with FcRγ and DAP12 in osteoclast lineage cells, we screened the expression profiles of messenger RNAs for known candidate receptors using GeneChip analysis. We found that a series of receptors and ITAM-associated molecules, as well as FcRγ and DAP12, are expressed in the osteoclast lineage (Supplementary Fig. 3a). These putative FcRγ- and DAP12-associating receptors[11-15] were detected on the surface of the osteoclast lineage using cell-surface labelling with biotin (Supplementary Fig. 3b, c). Among these, immunoprecipitation experiments confirmed that paired immunoglobulin-like receptor (PIR)-A, FcγRIII and OSCAR each pair with FcRγ and that triggering receptor expressed by myeloid cells (TREM)-2 and signal-regulatory protein (SIRP)β1, but not NKG2D, pair with DAP12 in the osteoclast lineage (Fig. 3c).

To test whether these receptor-mediated signals promote osteoclast differentiation by associating with FcRγ or DAP12, we stimulated BMMs with plate-bound monoclonal antibodies against OSCAR, PIR, TREM-2 and SIRPβ1. Triggering of either receptor by crosslinking with an antibody accelerated RANKL-induced osteoclast differentiation, indicating that these receptors activate osteoclastogenesis, although the stimulatory effect is more obvious at a low concentration of RANKL (Fig. 3d and Supplementary Fig. 3d). In the absence of RANKL, the stimulation of these receptors alone could not induce osteoclast differentiation (data not shown), suggesting that these receptor-mediated signals act cooperatively with RANKL but cannot substitute for the signal.

A stimulating effect by anti-OSCAR and anti-PIR antibodies was not observed in *FcRγ*$^{-/-}$ BMMs, whereas anti-TREM-2 and anti-SIRPβ1 antibodies stimulated *FcRγ*$^{-/-}$ BMMs, the same as they did with wild-type cells (Fig. 3e). This indicates that FcRγ is required for the stimulatory function of OSCAR and PIR-A. Consistent with the observation that osteoblasts rescue DAP12 deficiency through FcRγ-associated receptors, anti-OSCAR and anti-PIR antibodies could rescue the osteoclastogenesis from *DAP12*$^{-/-}$ BMMs but not from *DAP12*$^{-/-}$ *FcRγ*$^{-/-}$ cells (Fig. 3f). Stimulation of DAP12-associating receptors such as TREM-2 and SIRPβ1 did not rescue *DAP12*$^{-/-}$ BMMs. This indicates that DAP12 is required for the stimulatory effect through TREM-2 and SIRPβ1 (Fig. 3f).

How does the ITAM signal contribute to RANKL-induced signalling events? To address this question, we performed a genome-wide screening of mRNA expression in RANKL-stimulated

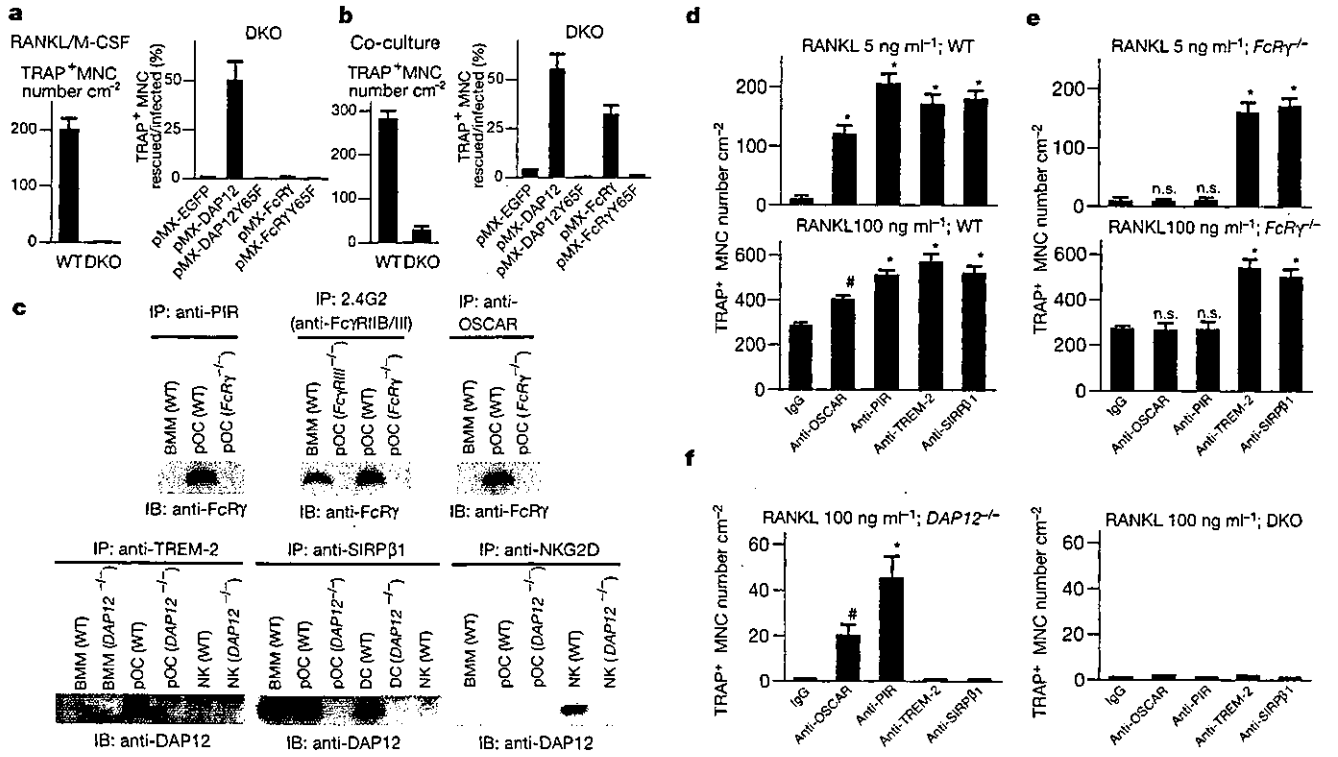

Figure 3 Distinct roles of FcRγ- and DAP12-associating immunoreceptors in the regulation of osteoclastogenesis. **a**, Complete block of *in vitro* osteoclastogenesis in *DAP12*$^{-/-}$ *FcRγ*$^{-/-}$ (DKO) cells stimulated with RANKL and M-CSF. This was rescued by pMX-DAP12, but not pMX-DAP12Y65F or pMX-FcRγ. **b**, Severe impairment of osteoclastogenesis in *DAP12*$^{-/-}$ *FcRγ*$^{-/-}$ cells even in co-culture with osteoblasts. Osteoclastogenesis was rescued by pMX-DAP12 or pMX- FcRγ in an ITAM-dependent manner. **c**, Association of FcRγ with PIR-A, FcγRIII and OSCAR (upper). pOC, osteoclast precursor cells stimulated with RANKL. For the comments on the association of FcRγ with FcγRIII, see Supplementary Fig. 3b, c. Association of DAP12 with TREM-2 and SIRPβ1, but not with NKG2D, in pOC (lower). For the positive control, DAP12 associates with SIRPβ1 and NKG2D in dendritic cells (DC) and NK cells (NK), respectively. **d**, Treatment of BMMs with plate-bound monoclonal antibodies against OSCAR, PIR, TREM-2 or SIRPβ1 promotes osteoclastogenesis stimulated by RANKL and M-CSF. The stimulatory effect by antibody-mediated crosslinking is more obvious at a low concentration of RANKL (5 ng ml^{-1}) than at a high concentration (100 ng ml^{-1}). **e**, Effect of plate-bound antibodies on osteoclastogenesis from *FcRγ*$^{-/-}$ BMMs. Anti-OSCAR and anti-PIR antibodies have no effect on *FcRγ*$^{-/-}$ BMMs. **f**, Effect of plate-bound antibodies on osteoclastogenesis from *DAP12*$^{-/-}$ BMMs or *DAP12*$^{-/-}$ *FcRγ*$^{-/-}$ cells stimulated with RANKL/M-CSF. Anti-OSCAR and anti-PIR antibodies rescued osteoclastogenesis from *DAP12*$^{-/-}$BMMs, but such an effect was not observed in anti-TREM-2 or anti-SIRPβ1 antibodies. No stimulatory effect was observed on osteoclastogenesis from *DAP12*$^{-/-}$ *FcRγ*$^{-/-}$ cells.